Using Simulated Clusters to Analyze and Develop Snow Radar Products in Grand Mesa, Colorado

©2022

Haejo Kim

B.S. Earth Science, University of California, San Diego, 2017

Submitted to the graduate degree program in Department of Geography & Atmospheric Science and the Graduate Faculty of the University of Kansas in partial fulfillment of the requirements for the degree of Master of Science.

David Braaten, Ph.D., Chairperson

Committee members

Nate Brunsell, Ph.D.

Josh Roundy, Ph.D.

Date defended: May 6, 2022

The Thesis Committee for Haejo Kim certifies
that this is the approved version of the following thesis :

Using Simulated Clusters to Analyze and Develop Snow Radar Products in Grand Mesa, Colorado

David Braaten, Ph.D., Chairperson

Date approved: May 6, 2022

Abstract

Obtaining timely basin-scale winter and early spring characteristics of snowpack in the Western United States are important for modeling water availability during the melt season, especially with increased warming due to anthropogenic climate change. Using an ultra-wideband (UWB) frequency modulated continuous wavelength (FM-CW) airborne radar sensor (2-18 GHz), we are able to map snow depth to an accuracy of 3 cm or less on a basin scale. The assessment of snow depth from processed radar data requires careful quality control, with precision of the assessment directly related to the time committed to the quality control effort. Given the inherent snow depth variability within a radar footprint (approximately 7m by 70m), a level of precision exceeding the inherent snow depth variability would needlessly delay the preparation of our snow depth data product. To quantify what level of precision is needed, we aggregated in situ snow depth measurements into clusters of similar dimensions to a radar footprint. We also examined how forest canopy and topology changes snow depth variability within a radar footprint, which parameters such as elevation, canopy heights or tree canopy cover drive snow depth variability, and whether these parameters are apparent in radar-derived measurements. We used in situ and radar measurements from Grand Mesa, Colorado, an extensively studied site for snowpack monitoring. We measure that snow depths in a 7 m by 70 m area can vary anywhere between 5% to 30% of the average snow depth of the footprint. Radar-derived snow depths were measured to be within these levels on variability (17% to 20%). Elevation is noted to be the primary driver of snow depth variability in Grand Mesa, followed by canopy heights and tree canopy cover from a randomforest regression. Despite limited availability of flight paths to analyze, this study showed good agreements of radar-derived snow depths to aggregated in situ snow depth variability.

Acknowledgements

I would first like to extend my gratitude to my advisor, Dr. David Braaten for giving me the opportunity to pursue graduate research here at the University of Kansas. Thank you for sharing your knowledge and being my mentor and advisor during the last two years.

I would also like to extend my thanks to the other members of my committee Dr. Josh Roundy and Dr. Nate Brunsell for their patience, support, and advice. I would also like to thank the faculty at the Remote Sensing Center at the University of Alabama, especially Dr. Drew Taylor and Omid Reyhani.

I also could not have done this and completed my masters without the help of the friends that I've made here in Kansas. Thank you to all of my peers, faculty, and staff both at CReSIS and the Atmospheric Science Department. The last two years that I have spent at KU and at Lawrence have been so memorable, and thank you all for your help.

Last but not least, I would like to thank my family for their unending support and love in pursuing my goals during these difficult times.

Contents

List of Figures

List of Tables

Chapter 1

Introduction

Seasonal snowpacks are an important resource of water and control the hydrologic cycle of the western United States and other regions around the world. Over 1.2 billion - approximately one sixth of the world's population - including at least 60 million people in the western United States rely on snowpack and glaciers as their main water supply for drinking and agriculture (Bales et al., 2006; Barnett et al., 2005; Sturm et al., 2017). Alpine snowpack acts as a natural reservoir of water during winter and early-spring that often exceeds man-made storage where it becomes the dominant source of water for the arid summer months (Mote et al., 2005; Serreze et al., 1999). Hydrological modeling has shown 53% of the total runoff in the western United States originates from snow, and accounts for over 70% of the runoff in the three major mountain ranges of the region (74% in the Rockies, 73% in the Sierra Nevadas, and 78% in the Cascades) (Li et al., 2017). Forecasting the subsequent snowmelt and runoff is now a crucial task that has been limited by available accurate spatial and temporal snowpack measurements (Jonas et al., 2009).

Snow is one the main sources of water in the western United States that plays a vital role ecologically and for human needs. Snow plays a role in land-atmosphere interactions and heat/energy redistribution by increasing the Earth's albedo and insulating soil from the atmosphere (Zeng et al., 2018). Snow's high albedo reflects some of the incoming short-wave radiation and provides enhanced cooling critical to the Earth's heat budget. Global snow covered area is approximately 1.9×10^7 km^2 and reflects at least 2×10^{12} GJ of energy (Sturm et al., 2017). The water produced from snowmelt controls the magnitude and timing of river discharge where it replenishes groundwater and reservoirs which is used for human consumption, agricultural use, hydroelectric power, and controls soil moisture and vegetation (Li et al., 2017; Sturm et al., 2017; Barnett et al., 2005;

Zeng et al., 2018). Accurate snow forecasting/monitoring is also needed for the role snow plays in our economy through jobs, winter tourism, and flood control (Carroll et al., 2006). As a result, the need for accurate information on snowpack conditions in real-time is crucial in making optimized decisions to meet and balance all of the demands.

Anthropogenic climate change has placed a historically strained water source under greater stress. Current Intergovernmental Panel on Climate Change (IPCC) projections of global mean surface air temperatures show an increase between 1 to 1.4 °C in the near term (2031-2050) and between 1 to 3.7 °C at the end of the century (2081-2100) depending if global greenhouse gas emissions are curbed (IPCC, 2019). These trends were also reported in the Fourth National Climate Assessment (NCA4) where much of the United States will observe warmer temperatures (Reidmiller et al., 2018). Precipitation redistribution will also occur where much of the US Southwest can potentially face less rain and snow and increased evaporation (Reidmiller et al., 2018; Seager et al., 2007). Water availability is projected to be increasingly important as demand for water is slated to increase and a diminishing water resource with decreasing snow and increased evaporation compound this problem. Research and development has been undertaken to create models like the operational National Water Model (NWM) to create forecasts for floods and water measurements. For many of the snowmelt fed river basins, accurate snow measurements helped to improve model predictions in the NWM forecasts.

The increased warming has had a negative impact on snow resources both globally and in the western United States. Zeng et al. (2018) found the snow season defined from the day of first snow water equivalent (SWE) measurement and day of last SWE measurements, has shortened from 1982 to 2016 at a rate of -1.22 days/year in the Colorado River Basin and -0.97 days/year over the western conterminous United States, totalling an average decrease in the snow season of 34 days mainly due to an increase in temperature. Zeng et al. (2018) also found a negative trend in snow mass with annual maximum SWE decreased by 41%. Peak snowmelt runoff has been observed and modeled to occur about 4 weeks earlier (Mote et al., 2005; Stewart et al., 2005). Combined with an aging infrastructure and not enough reservoir storage capacity, most of the early snowmelt

is lost to the ocean (Sturm et al., 2017). Warming temperatures have also corresponded to less snowfall during winter with the number and intensity of winter snowfall events decreasing, and a notable redistribution in precipitation patterns (Knowles et al., 2006; Dettinger et al., 2015; Sturm et al., 2017). Snow-covered area over land has also been steadily decreasing which is consistent with a warming climate (Sturm et al., 2017). A decrease in snow-covered areas has shown to increase average annual and spring temperatures by at least 2-4 °C due to less cooling from the snow-albedo feedback (Diro & Sushama, 2020). All of these trends work to change snowmelt timing which creates a mismatch between water availability and water need where some early melt water is lost to oceans due to insufficient storage, reduced stream runoff from increased winter rain, and decreased cooling from reductions in snow-covered areas (Sturm et al., 2017).

The loss of snow resources also has societal impacts. Areas that depend on winter sports and tourism are starting to face losses with a loss of at least $1 billion and 17,400 jobs per year between 2001 and 2016 (IPCC, 2019) in the United States. Projected revenue losses near the end of the century (2090) could top $2 billion in ticket sales and day fees alone (not including lodging, transport, etc.) using the worse case scenario of the current IPCC projections of warming (IPCC, 2019). Agriculture would also be heavily affected by the lack of water in spring/summer where current annual losses range between $1 billion to$ 1 trillion, with the lower end of the range increasing to over $0.5 trillion in losses over the next few decades (Sturm et al., 2017). All of these negative impacts have increased the demand for accurate monitoring of snow pack and runoff.

Effective water resource management is also dependent on the skill and precision of hydrological models. Results of both short term forecasts (2 day) and long term forecasts (2 years) are needed to fulfill all needs (Blum & Miller, 2019). Good forecasting of snow water content is important for both of these times scales. Flooding damages from rain-on-snow effects (McCabe et al., 2007) have been well documented and long term forecasting of water has been discussed above. Understanding critical trends in snow water availability is reliant on good information of the SWE of the snowpack, followed by snow depth/thickness. Remote sensing techniques have been developed to help improve monitoring of snowpack over broad areas. However, as Sturm

et al. (2010) pointed out, most passive microwave satellite platforms have had success in reporting snow cover area, but has had difficulty in reporting both snow depths and SWE in a variety of conditions (i.e., wet snow). Airborne lidar or gamma ray surveys have had some success in reporting snow depths and/or SWE, but are limited in spatial extent. Research has been conducted on an airborne platform for an ultra-wideband (UWB) frequency-modulated-continuous-wavelength (FM-CW) radar known as the Snow Radar. The Snow Radar has been shown to be more robust than satellite platforms using passive microwave sensors and differential methods using altimeters, and shows good agreement with in situ measurements (Yan et al., 2017b). This study will focus on the current version of the Snow Radar operating over a frequency range of 2-18 GHz.

This work analyzes and verifies snow measurements obtained using a Snow Radars in an alpine environment. A footprint analysis is used to verify the snow depths measurements from the Snow Radar against ground-based measurements. These footprints will also be used to look at how the forest canopy affects snow depths. Finally, this study will take these results and create a regression model to validate these results. Chapter 2 provides a review of the factors that affect snow depths and a review of the methods of obtaining snow depths. Chapter 3 describes the observations and methods used. Chapter 4 presents the results of the study, and Chapter 5 concludes the study and presents possible future work.

Chapter 2

Background

2.1 Factors of Snow Depths

Characteristics of snow and seasonal snowpack depend on the environment that it exists in. Remote sensing of seasonal snow has remained a constant challenge in accurately and consistently measuring snowpack characteristics over a diverse range of conditions and landscapes (McGrath et al., 2019). The difficulty of measuring snowpack properties is compounded by its high natural spatial and temporal variability. These spatial and temporal variabilities can occur at a wide variety of scales. For example, snow depths can be dependent on small-scale vegetation and surface roughness to large-scale terrain features or meteorological precipitation patterns (Elder et al., 1989, 1991). Snowpack formation is largely controlled and explained by two processes: accumulation and ablation. Typically, accumulation processes are dominate between October to March and ablation processes are dominate between April to June but, combinations of these processes can complicate alpine snowpack monitoring.

The important variables for snow depths in an alpine watershed identified by Elder et al. (1989) and Elder et al. (1991) were radiation, slope, and elevation. Across multiple studies, elevation has been discussed as one of the most important variables for snow depths. Since temperature largely decreases with height and precipitation increases with height, snow depth generally increases as elevation increases (Dingman, 1981). The relationship between snow depth and elevation was also found by Grünewald et al. (2014) in the Swiss Alps, where snow depths typically increased with elevation, but reach a peak value. Changes in elevations are also related to changes in topography which modifies the interactions between the snowpack and topography leading to the peak snow

depth values such as the preferential deposition of precipitation, redistribution of snow by wind, sloughing and avalanching (Grünewald et al., 2014). Wind redistribution in alpine environments is another known variable of snow depth variability, where accelerating (decelerating) or convergent (divergent) flows lead to accumulation (erosion) (Elder et al., 1991). Another study by Currier & Lundquist (2018) also noted that snow depth variability in Boulder Creek, Colorado was dominated by wind, where snowdrifts, areas of preferential deposition of physically blown snow, was found. Slope can control changes of significant volumes of snow. Steep slope angles cause snow to repeatedly slough, as avalanches can move large volumes of snow (Elder et al., 1991).

Along with physical variables, energy balance is also a factor in snow depth variability. Energy inputs and outputs at the air/snow and snow/ground interfaces can be affected by incoming/outgoing radiation, sensible and latent heat exchange, heat flux from the ground, and advective heat transfer, but is dominated by solar and longwave radiation (Elder et al., 1991). Melting from radiation typically reduces snow depths and increases density but not SWE, if the melt percolates through the snowpack and refreezes (Elder et al., 1991). The amount of melting is also dependent on physical characteristics of the environment such as slope, aspect, and latitude which will modify radiation inputs, and parts of an alpine basin may experience a period of up to two months without receiving direct insolation while adjacent areas my receive direct radiation (Elder et al., 1991). Snow sublimation has also been found to be important in explaining alpine snowpacks. Snow sublimation comes in three main forms: surface sublimation between the air/snow interface, canopy sublimation from intercepted snow held in the forest canopy, and blowing snow sublimation (Sexstone et al., 2018). Ignoring sublimation in snow models can overpredict snow depths, where sublimation losses were quantified to between 10-20% in large valley areas and mountain slopes, 50% in dense canopy stands, and up to 90% at peak mountain crests of the total seasonal snowfall (Strasser et al., 2008). When accounting for the scale of these processes in a basin, modeled losses relative to the the total snowfall from surface sublimation, canopy sublimation, and blowing snow sublimation were found to be -6.9%, -13.0%, and -4.1% respectively (Strasser et al., 2008). Another important factor in sublimation which is often neglected in the water budget is

ground resublimation into a hoar frost (freezing dew) layer has been modeled to 2.4% of the total snowfall (Strasser et al., 2008).

Vegetation also plays a significant role in modifying snow accumulation and ablation. It is approximated that 20% of the Northern Hemisphere seasonal snowpack exist under forested environment that creates microclimates affecting snow depth variability (Malle et al., 2019). Forest canopy will modify both physical and energy balance processes where shortwave radiation, precipitation and wind speeds are reduced while longwave radiation and humidity are enhanced which are affected by differences in surface albedo and latent heat fluxes between open and covered snowpack (Strasser et al., 2008; Malle et al., 2019). As mentioned previously, forest canopy also increases the sublimation of snow in two main ways: through latent fluxes at the surface and from physically intercepted snow in the forest canopy which sublimates back into the atmosphere (Strasser et al., 2008). These modifications to snow accumulation and ablation by the forest canopy leaves a distinct spatial signal identified by Musselman et al. (2008) called tree wells with reductions up to 47% of the snow depths just due to canopy interception. In addition to variability under the forest canopy, significant changes to the snowpack also exist around forest edges. Musselman et al. (2008) also noted there was a 25% increase in snow depths on the north side of trees as a result of shading. Along with interactions from the canopy, snow depth variability was found along forest edges as a result of vegetation distribution. Currier & Lundquist (2018) compared snow depths differences on forest edges across the western United States. Specifically for sites in Colorado, a statistically significant difference in the windward vs leeward forest edge snow depths of 38% of the median was found. A similar north/south difference in snow depths as described in Musselman et al. (2008) was found for Boulder Creek at the forest edges but was not statistically significant. This deposition was found to be wind-related where colder temperatures, strong westerlies, and the presence of ribbon forests acting like wind breaks led to higher snowdrifts on the leeward side of forests (Currier & Lundquist, 2018).

Snow density is another important metric to consider for snowpack monitoring especially for calculation of SWE. Typically, in most alpine environments, snow depths has more variability

compared to snow density, and is the major source of variability of SWE (Elder et al., 1989, 1991). Snow density variability is also subject to change throughout the year, and also highly variable between water seasons as well. As noted by Elder et al. (1991), during the 1987 water year at the Emerald Lake watershed in northern California, snow densities were low at the beginning of February and early March due to colder conditions but rose as temperatures warmed through March and April. The standard deviations of snow density during February and early March of 1987 was also low since the snowpack was cold and homogeneous, but rose in March due to heterogeneous zones of cooling and warming, before dropping abruptly in late March and April before the onset of melting (Elder et al., 1991). This was contrasted to the 1986 water year, where snow density was highly uniform (Elder et al., 1991). Snow density can change due wind erosion, melting and refreezing events, compaction, and snow metamorphosis typically changing grain sizes (Bormann et al., 2013). Higher snow densities are typically a factor of high precipitation, warmer temperatures, stronger winds, and long season duration (Bormann et al., 2013). Another important factor to consider about snow density is also the variability vertically throughout the profile of the snowpack. Vertical changes in snow density are the result of compaction from the weight of new snow, internal gradients of moisture and temperature, as well as formations of ice and hoar frost layers (Bormann et al., 2013). Obtaining snow density measurements is a labor-intensive and time consuming process where a snowpit has to be excavated and samples are taken from the pit wall at regular intervals to create a density profile (Elder et al., 1991), or else a mean snow density measurement can be taken from instruments like a federal snow sampler as discussed in the next section. While snow density is an important factor to consider, this study will focus on snow depths due to the lack of snow density measurements at high resolutions from in situ sources.

2.2 Snow Measurements

2.2.1 Field Surveys and Remote Sensing

Seasonal snowpack has remained a constant challenge to accurately and consistently measure. Observations of snowpack properties like snow depths and SWE rely on in situ field surveys (Figure 2.1). In a field survey, snow depths can be robustly probed while density measurements involve labor-intensive and time-consuming excavations of snowpits (Elder et al., 1991). With depth gauges, ground-based surveys can cover 10's of km^2 and collect hundreds of measurements. These seasonal surveys can use rudimentary instruments like the avalanche poles (Figure 2.1). Federal snow tubes (Doesken & Judson, 1997, pg 51) shown on Figure 2.3b are hollow tubes that can inserted into the snowpack to extract a core samples that can be weighed, so SWE and snow depths can be recorded simultaneously (Sturm et al., 2010; Dressler et al., 2006). Marshall et al. (2006) and Sturm & Holmgren (2018) also described newer instruments like the MagnaProbe (Figure 2.2), an automatic snow depth probe with an integrated GPS, that can obtain 10x more depth measurements than an avalanche pole. The United States has historically conducted monthly snow course surveys since the 1930s. A snow course is a permanent site approximately 300 m long (1000 ft) where measurements of snow depths and SWE using federal snow tubes are made for a snowpack at a known elevation. Typically, one snow depth and SWE measurement is reported at the beginning of each month from January to June to represent the average of 10 measurements made on the course (Dressler et al., 2006). In very remote areas or during dangerous conditions, snow course measurements can be made on an airborne platform through aerial markers (Figure 2.3a), which are giant "rulers" where snow depths can be visually read from a distance.

The gaps in snow data occur because manual sampling can be expensive, dangerous, and time-consuming (Deems et al., 2013). Avalanche hazards must be considered in areas with steep slopes. Further gaps in ground stations especially at high elevations compound the problem (Behrangi et al., 2018). Despite these downsides and dangers, field surveys are still an essential method to compare against remotely sensed or modeled snow depths and have been used continually in the

Figure 2.1: Image of depth measurement from Jan 2020 field survey of snowpack in Grand Mesa, Colorado using a 3 m avalanche pole.

literature. Clow et al. (2012) used snow surveys to compare with the National Weather Service's Snow Data Assimilation (SNODAS) estimates. López-Moreno et al. (2013) used snow surveys to use regression models to estimate the spatial variation in SWE and snow density in the Spanish Pyrenes mountains. Guyennon et al. (2019) also used a similar method for snowpack in the Italian Alps.

In order to increase the number of snow measurements, automated snow stations were placed across the Western United States through United States Department of Agriculture (USDA) National Resources Conservation Services (NCRS) SNOw TELemetry (SNOTEL) network. Over 800 stations were placed in remote areas often replacing snow courses that were dangerous or ex-

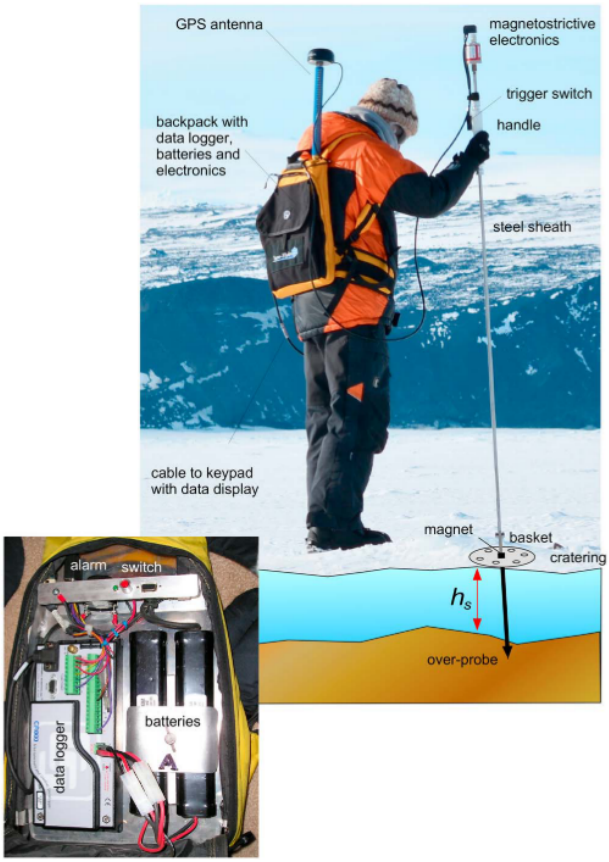

Figure 2.2: Magnaprobe in use in the field. Snow depths are measured from the floating basket to the tip of the probe where it can be logged by the data logger found in the backpack along with batteries and a GPS. Image taken from Sturm & Holmgren (2018).

pensive, and were designed to be fully automated outside of a basic service to reset the instruments (Serreze et al., 1999; Dressler et al., 2006). An example advanced SNOTEL station is shown on Figure 2.4a with the instruments labelled. The basic measurements made on SNOTEL stations are air temperature, precipitation, snow depths, and SWE measurements at hourly, daily, and monthly time scales, but more advanced stations also measure soil moisture, wind, and radiation. Currently the NCRS still operates and collects data from both snow course sites and SNOTEL stations. Snow depths were measured in multiple ways on SNOTEL stations, but automated snow depths are made using an ultrasonic snow depth sensor (from https://www.nrcs.usda.gov). Precipitation accumulation is collected with gauges designed to maximize catch efficiency which are charged with an anti-freeze solution to mitigate freezing and evaporation and stored for the entire year where the

(a) Aerial Marker

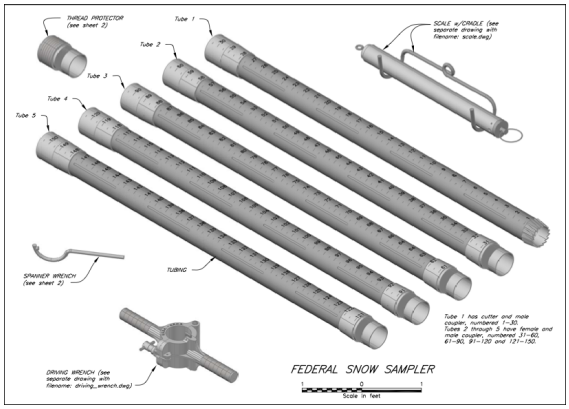

(b) Federal Snow Tube

Figure 2.3: (a) An example of an aerial ground marker where snow depth measurements can be made from an aircraft. (b) Example of a Federal Snow sampler, a hollow tube that can extract a column of snow. The filled tube can be weighed to make an estimate for density which is used to calculate SWE. All images were taken from wcc.nrcs.usda.goc/snow/

amount of precipitation is measured through a pressure transducer (Serreze et al., 1999). SWE is measured using a snow pillow, a pressure sensor where accumulating snow induces height changes in a manometer with an anti-freeze solution (Serreze et al., 1999; Dressler et al., 2006).

Several drawbacks to SNOTEL SWE measurements have been identified due to instrument design. The snow pillow is subject to erroneous measurements which can be formed as a result of ice-bridging across the instrument and environmental factors such as debris or snow drifting (Fassnacht et al., 2003), but is often unidentifiable from errors in instrument sensitivity (Serreze et al., 1999). Johnson & Schaefer (2002) also found similar errors in snow pillow measurements where under- and over-measurements were a result of differences in snow shear strength leading to bridging or extra load from surrounding snow. These errors were found to be more common during the transition from winter to spring where different heating tendencies from the snow pillow and

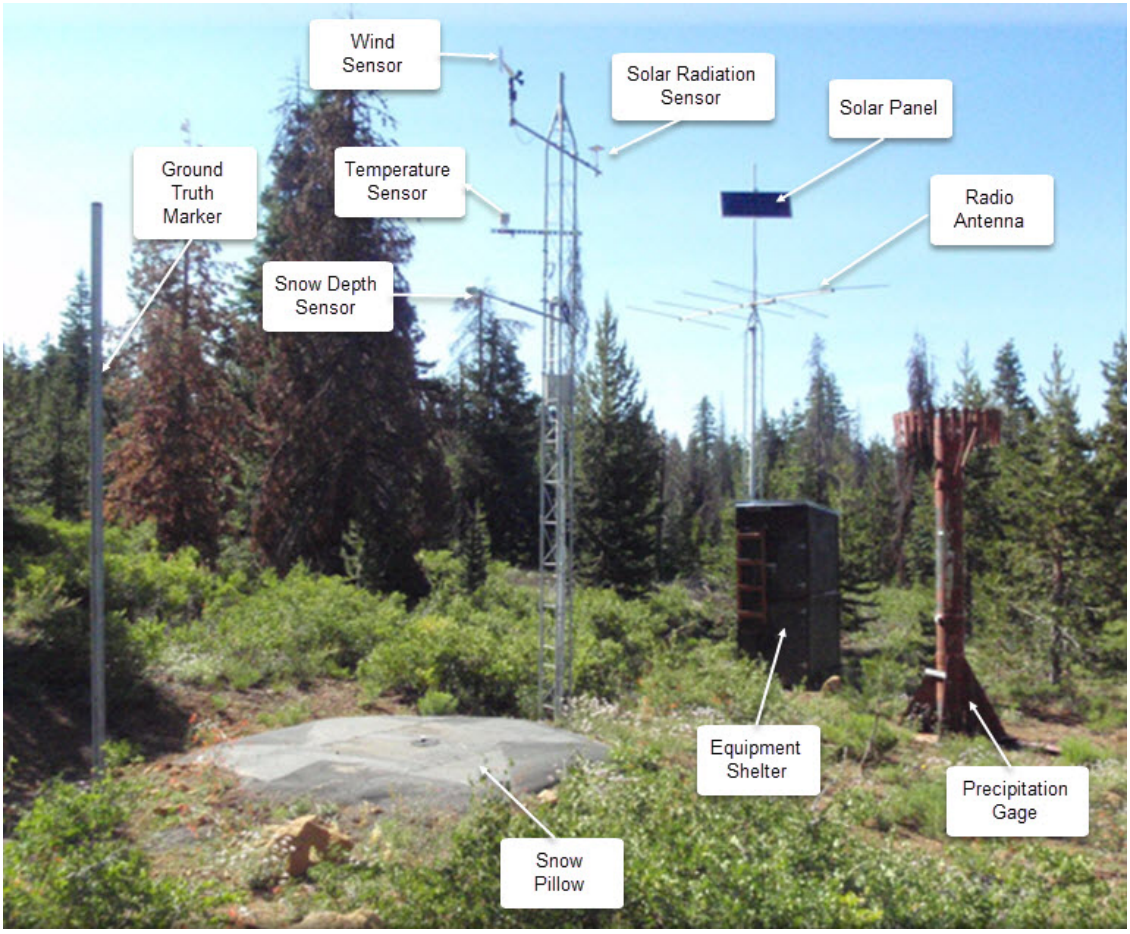

(a)

(b)

(c)

Figure 2.4: (a) An example of a SNOTEL site with instruments labelled. Instrumentation and data availability are different from station to station depending on data demand. Examples of SNOTEL stations on Grand Mesa are shown: (b) Mesa Lakes and (c) Park Reservoir. All images were taken from wcc.nrcs.usda.goc/snow/

the ground are more pronounced to errors. Quality control regimes were developed to correct erroneous SWE measurements by removing values that exceed five standard deviations from a monthly average (Serreze et al., 1999) or correcting SWE using reference snow density and snow depths at the time of error (Johnson & Marks, 2004). Additionally, despite being densely sampled, only small portions of snow covered areas in the western United States are sampled by SNOTEL or snow courses where sensor density is approximately 1 for every 700 km^2 in the Sierra Nevada (Oaida et al., 2019). Higher elevations are also undersampled by these methods, where the majority of measurements are made between 1900 and 2900 m, where snow tends to be concentrated during drier years or at the end of the snow season (Oaida et al., 2019). Grand Mesa has two SNOTEL sites that can be used as additional ground observations to compare against radar measurements and provide quality control.

Outside of snow markers visible from aircraft, one method of airborne remote sensing currently in operational use in the United States is through detection of gamma rays. The National Oceanic and Atmospheric Administration's (NOAA) National Operational Hydrologic Remote Sensing Center (NOHRSC) has been making airborne gamma SWE measurements for 40 years starting in 1979 and helps to support an operational high resolution snow model (Cho et al., 2020). The NOHRSC maintains over 1900 flight lines across 29 states and 7 Canadian provinces (Carroll, 2001). Natural terrestrial gamma radiation are released by radioactive isotopes of potassium, uranium, and thorium primarily in the upper 20 cm of soil. This gamma ray radiation is attenuated by any phase of water and is used to estimate SWE directly. This radiation is measured using a low-flying aircraft (150 m) across multiple flights where measured differences in radiation can be used to make a mean areal SWE estimate from surveys of bare ground and snow covered ground. The relationship between SWE and this radiation from Carroll (2001) was:

$$SWE = \frac{1}{A}\left[\ln\frac{C_0}{C} - \ln\frac{100+1.11M}{100+1.11M_0}\right] \tag{2.1}$$

where C and C_0 are terrestrial gamma counts over snow and bare ground respectively, M and M_0

are percent soil moisture over snow and bare ground respectively, and A is a radiation attenuation coefficient. Three SWE measurements are made from gamma fluxes of potassium, thallium, and gross counts (GC). A singular weighted SWE measurement is calculated:

$$SWE_{gamma} = 0.346 \cdot SWE(K) + 0.518 \cdot SWE(Tl) + 0.136 \cdot SWE(GC) \tag{2.2}$$

which is reported for the entire flight line. A typical flight line for gamma measurements have a swath of 300 m and are 16 km long. Sources of errors in gamma SWE estimates have been summarised by Cho et al. (2020) as:

1. Current operational approach assumes no changes in soil moisture from the bare ground surveys, however, soil moisture can change after these surveys due to precipitation events.

2. Forest biomass has been noted as a source of error. Deep snowpack are more heavily affected where attenuation of terrestrial gamma radiation by snowpack may be thwarted by forest biomass above the deep snowpack.

3. Variability in shallow and deep snowpack causes an "uneven snow effect" due to very uneven terrain or snow drifting.

Another issue of gamma ray surveys can come from its lower altitude flights. Lower flights cannot be used in uneven terrain.

Another common airborne remote sensing technique used in the literature was lidar altimetry. A prominently featured platform is the National Aeronautics and Space Administration/Jet Propulsion Laboratory (NASA/JPL) Airborne Snow Observatory (ASO) which uses a combination of an imaging spectrometer and a scanning lidar (Painter et al., 2016; Behrangi et al., 2018). The ASO is able to survey large mountainous basins in California, Nevada, and Colorado approximately 1000 km^2. For example, the Tuolumne River Basin in northern California was first surveyed by the ASO in 2013 and was 1,180 km^2 (Hedrick et al., 2018). Since then, the ASO conducted surveys for river basins providing snow depth measurements and SWE products at 3-m and 50-m resolutions respec-

tively. Snow depths are calculated by taking a difference between elevations taken when snow is present with a baseline snow-free elevation survey. The ASO can then make scheduled runs at weekly or monthly intervals. A typical turnaround period for SWE products is 24 hours from the moment of the aircraft lands (Hedrick et al., 2018). ASO measurements of snow depths for the 3 m spatial resolution have mean absolute errors of < 8 cm and biases < 1 cm, that decreased with the 50 m spatial resolutions (Painter et al., 2016). Uncertainties in SWE was a function of the uncertainty in snow densities (13-30 kg m^{-3}) and snow depths were relatively unbiased (< 0.02 m at 50 m resolution) (Painter et al., 2016). Behrangi et al. (2018) showed satellite and ground radar products typically underestimated snow depths when compared to ASO measurements, but had high correlations (>0.8) at the monthly scale in the Sierra Nevada.

Remote sensing techniques on satellite and airborne sensors have been used to fill gaps in snow data. One common satellite sensor is the AMSR/AMSR-E onboard Aqua and currently on the JAXA GCOM-W1 satellite (Tedesco & Narvekar, 2010). Retrieval of SWE and snow depths through passive microwaves are similar to how gamma rays were measured where microwaves naturally emitted from the soil is attenuated by the snowpack (Tedesco & Narvekar, 2010). A baseline SWE retrieval algorithm was initially measured by a linear relationship between SWE and brightness temperatures (T_b) difference at 18 and 37 GHz.

$$SWE = R_c * \Delta T_b \tag{2.3}$$

The coefficient R_c was derived using fixed values of grain radius and density. Current algorithms for SWE retrieval takes an initial guess of snow depth from (T_b). A separate snow cover algorithm determines if snow is present and filters possible snow pixels and reprojected onto 25 km EASE-grid. Snow depths are calculated using:

$$SD = ff(SD_f) + (1 - ff) * (SD_o) \tag{2.4}$$

where snow depths (SD) is the total sample depth between snow depths for forested and unforested

areas (SD_f and SD_o respectively). The forest fraction (ff) is ancillary data that is used in the algorithm. The SWE is then calculated from the averaged snow depths in the EASE-grid and ancillary snow density measurements (snow densities can be normalized by the density of water to obtain SWE into [mm]) using the following equation:

$$SWE[mm] = SD[cm] * \rho_{snow}[gcm^{-3}] * 10.0[mm/cm] \tag{2.5}$$

Results showed poor correlations between the AMSR-E SWE and SNOw Data Assimilation System (SNODAS) SWE with the largest during November and December ($r \simeq 0.2$) and lowest in February ($r \simeq 0.1$) (Tedesco & Narvekar, 2010). Some of the issues and error sources of the retrieval algorithm summarized from Tedesco & Narvekar (2010) are:

1. During the snow season, grain size and snow density change due to melting and refreezing cycles. Changes in density and grain size as well as layering of fresh snow can change the microwave response from snow.

2. Passive microwave sensors like AMSR-E cannot reliably measure deep snowpacks. Deep snowpacks, greater than 200 mm SWE (Cho et al., 2020), cannot be measured because the attenuation of microwaves at the higher frequencies is too high.

3. Forests can also attenuate microwaves depending on fractional volumne, crown and stem closures, basal area, and foliage biomass which are all important modulators of (T_b).

4. The penetration depths is drastically reduced with the presence of liquid water. SWE cannot be reliably measured with the presence of liquid water, and also struggles with wet snow cover.

Another satellite that has been getting traction in the literature is the Sentinel-1 by Lievens et al. (2019). The Sentinel-1 satellites from the European Space Agency (ESA) uses a C-band sensor operating at 5.4 GHz with a revisit time of 6 days which are processed at a 1 km^2 resolution (Lievens et al., 2019). Sentinel-1 measures the co-polarized (vertical-vertical) and cross-polarized

(vertical-horizontal) C-band transmit-receive backscatter (Lievens et al., 2019). Snow depths are calculated if snow cover and fractional forest cover are detected through a snow index by calculating a change in the cross-polarization ratio. Snow depth retrievals from February 2018 had a spatial correlation of 0.76 with monthly averaged snow depths and showed better representation of snow depths vs elevation when compared with the MERRA-2 reanalysis data (Lievens et al., 2019). The average mean absolute error (MAE) can be between 0.18 m and 0.31 m depending on whether 0 snow depth values were included (Lievens et al., 2019). Sentinel-1 snow depth retrievals are not as limited as they are with the AMSR-E sensor which can be hampered in areas of complex topography and smaller snow depths (Lievens et al., 2019).

2.2.2 FM-CW Radars

Since the late 1970s, research and development of FM-CW radars has been used to research snow and glaciers. FM-CW radars were theorized as an alternative to passive microwave satellite platforms which have higher levels of difficulty retrieving snow depths and altimeters which can only be applied to very limited regions since it needs accurate elevation data and can be hindered by vegetation (Yan et al., 2017a). Yankielun et al. (2004), Marshall et al. (2006), and Panzer et al. (2013) cites multiple studies of FM-CW radars in snow and avalanche research starting in the 1970s and successfully operated on NASA aircraft since 2009. Historically, most FM-CW measurements were made on the surface. Some early airborne radars were placed on helicopters which flew at maximum altitudes of 20 m, not suited for complex mountainous terrains or alpine regions (Panzer et al., 2013; Yankielun et al., 2004). FM-CW radars have been shown to perform better than impulse radars with snow depths errors less than 10%, where the higher bandwidths allow for greater sensitivity and resolutions (Marshall et al., 2007).

A summary of the FMCW radar from Yan et al. (2017a) is described along with a block diagram of a generic FM-CW radar on Figure 2.5. A transmit signal called a chirp is generated by sweeping the input voltage of a voltage-controlled oscillator (VCO) and transmitted to the antenna. A portion of the chirp is also coupled to a receiver. The reflected signal is received off a target and coupled

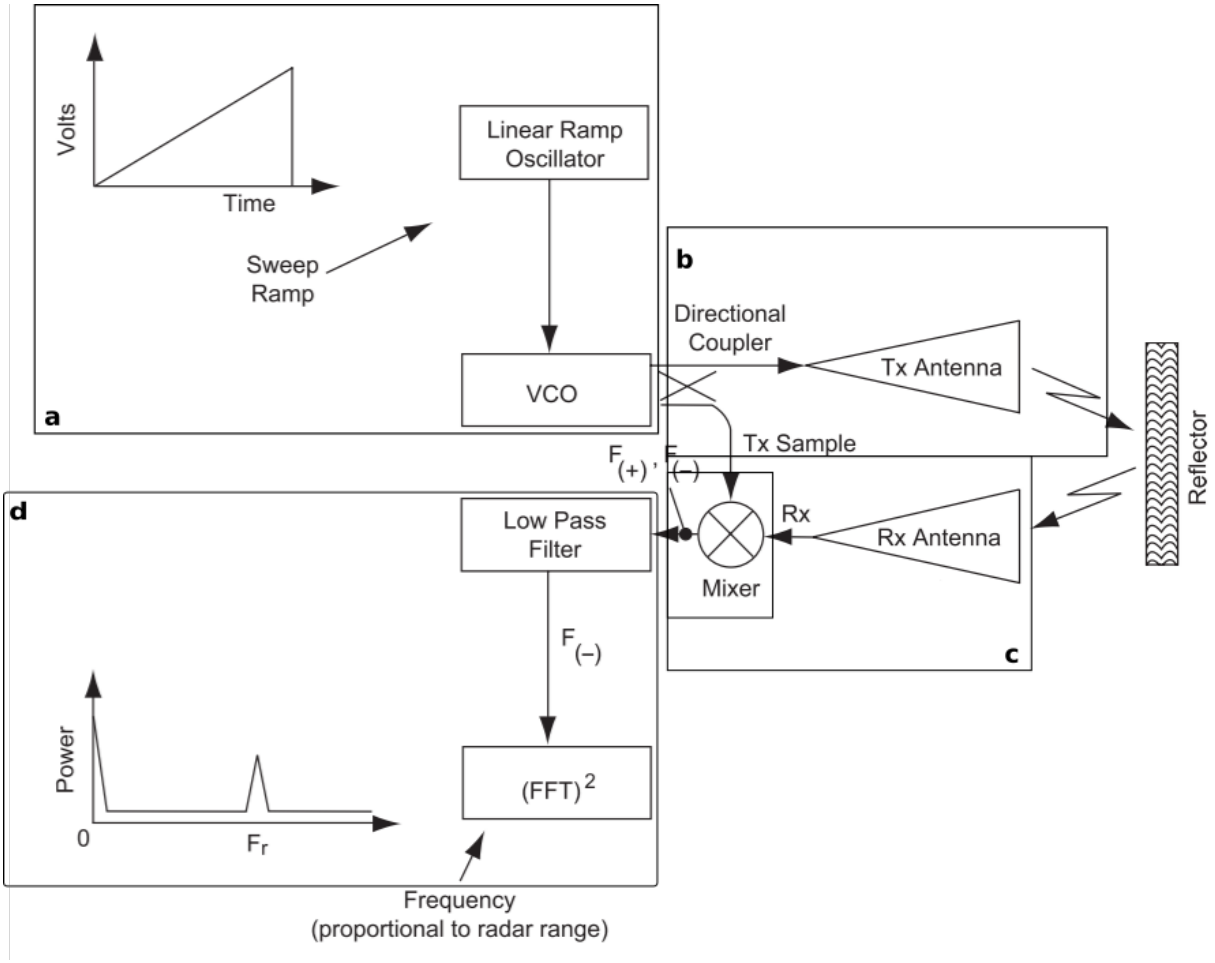

Figure 2.5: Block diagram showing the function of a generic FMCW radar taken from Yankielun et al. (2004). a) The transmit signal is generated by sweeping the input voltage into the voltage-controlled oscillator (VCO). b) A transmit signal is transmitted by a transmit antenna and to the receiver. c) A reflected signal is received and coupled with the transmit signal. d) A difference between the transmit and receive signal called the beat frequency is generated after being low-pass filtered.

to the receiver through a circulator, amplified, and mixed with the chirp. The product of the two signals is filtered to retrieve the frequency difference, called the beat-frequency signal (Figure 2.6). Snow depths are derived by measuring the time delay from the radar and changes in the dielectric constant along the path of the signal. For terrestrial snow, the greatest change in dielectric constants is found between the snow/ground interface and the air/snow interface. Snow depths can be determined by the propagation time delay between the air/snow and snow/ground interface assuming a dielectric constant of snow (1.53 for dry snow) and a snow density estimate. The

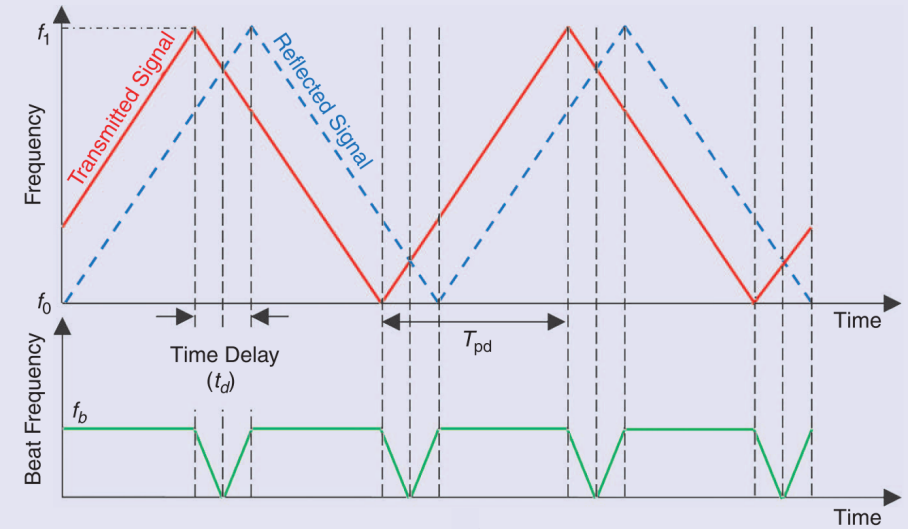

Figure 2.6: The beat frequency is generated by the difference in the transmitted signal (red solid line) and the reflected signal (blue dashed line) from Yan et al. (2017a)

uncertainty of snow depths is $\pm 6.63\%$ for a ± 0.1 gcm^{-3} variation in snow density.

Since the early 2000s, research and development of in-house UWB FM-CW radars has been conducted at the Center for Remote Sensing of Ice Sheets (CReSIS) at the University of Kansas (Panzer et al., 2013) and currently at the Remote Sensing Center at the University of Alabama (Yan et al., 2016b; Taylor et al., 2019; Yan et al., 2017b). Table 2.1 lists the parameters of different versions of the Snow Radar from 2003 to 2015 used in various missions. Early FM-CW radars were limited in frequency linearity and sweep rate of the chirp signal, which limited the range of the radars (Yan et al., 2017a). Since the first deployed Snow Radar in 2003, updates and improvements have been made to the Snow Radar over time. Results during the NASA Operation Ice Bridge (OIB) campaign of the 2-8 GHz Snow Radar and the 2-18 GHz Snow Radar showed good agreements with in situ data for snow over sea ice offshore from Barrow, Alaska. During the 2012 OIB survey, correlations between the radar-derived and in situ snow depths were 0.711 and 0.703 for two transects, and 0.89 for a 2015 survey using the higher bandwidth sensor (Yan et al., 2017a). Errors for each sensor were very similar with Root Mean Square Error (RMSE) of approximately 6 cm and Mean Absolute Error (MAE) between 4 to 5 cm. (Yan et al., 2017a). However, better performance was seen in the 2015 survey was observed where both RMSE and MAE both dropped

Table 2.1: Summary of the evolution of the Snow Radar as summarized from Yan et al. (2017a). Improvements were made to the Snow Radar before each field campaign.

Year Deployed	2003	2006, 2009	2010-2012	2013-2015	2015
Mission flown	AMSR-E	AMSR-E, NASA OIB	NASA OIB, NSF CReSIS	NASA OIB, NSF CReSIS	NRL, AWI
Airborne platform	N/A	P3, DC8	P3, DC8	P3, DC8, Basler	Twin Otter, Basler
Operating altitude	1 m	> 450 m	> 450 m	> 450 m	> 450 m
Operating frequency	2-8 GHz	2.5-7 GHz 4-6 GHz	2-6.5 GHz 2-8 GHz	2-8 GHz	2-18 GHz
Theoretical resolution	2.5 cm	3.3-7.5 cm	2.5-3.3 cm	2.5 cm	0.94 cm
Sweep time	10 ms	250 μs	250 μs	240 μs	240 μs
PRF[1]	25 Hz	2 kHz	2 kHz	3.9kHz	3.9 kHz

to 3.98 and 2.99 cm when data over the flat ice regions were considered alone (Yan et al., 2017a). Alpine snow measurements were also made using the Snow Radar in Grand Mesa in 2016. The radar derived snow thicknesses from a flightline ranged between 107 to 162 cm, and in situ values from the two SNOTEL stations at Grand Mesa were 117 cm and 147 cm on February 16, 2016 (Yan et al., 2016a). Currently, snow radars operating at a frequency range of 2-18 GHz are tested and used to obtain snow depths. A table of radar parameters are listed on Table 2.2. Overall, UWB FM-CW showed the ability to accurately measure both thin and thick snow thicknesses.

Table 2.2: Snow Radar parameters used for the 2019 and 2020 Grand Mesa surveys

Parameter	Value
Frequency Range	2-18 GHz
Bandwidth	16 GHz
Chirp Length	180 μs
PRF	4.35 kHz
Transmit Power	30 dBm
ADC Sampling rate[2]	1.2 GHz
ADC Resolution	14 bits
Range resolution	0.94 cm

[1] Pulse Repetition Frequency
[2] Analog-to-Digital Converter (ADC)

Chapter 3

Methods

The main goal of the study is to demonstrate the ability of the Snow Radar to provide timely data to use for hydrological models, research, and water resource management. In order to provide timely data for operational use, some trade-offs must be made such as precision for calculation speed. This study aims to first quantify the level of precision needed for Snow Radar measurements within its footprint area of 7m by 70m by answering the following research questions: What is the natural variability of snow depths within the specified dimensions of the footprint, and how does this variability change with respect to topological changes and especially vegetation? What are the main drivers of snow depth change in an environment? Are the Snow Radar measurements within acceptable margins compared to the in situ measurements?

3.1 Study Area and Data

In order to address the research questions, this analysis will compare snow depths from Grand Mesa, Colorado - a forested study site approximately 40 miles east of Grand Junction - from several different sources: ground-based snow surveys and remotely sensed data. A map of the study area is provided in Figure 3.1. Grand Mesa is a heavily studied region for remotely sensing snowpack such as NASA's multi-year SnowEx Campaign. Grand Mesa was primarily chosen to focus on how forests affect remotely sensed snow measurements without other compounding factors such as complex terrain (Kim et al., 2017).

The primary snow depth measurements focused in this study are from ground based surveys conducted in mid-winter Mar 2019 and Jan/Feb 2020. We conducted surface-based fieldwork in

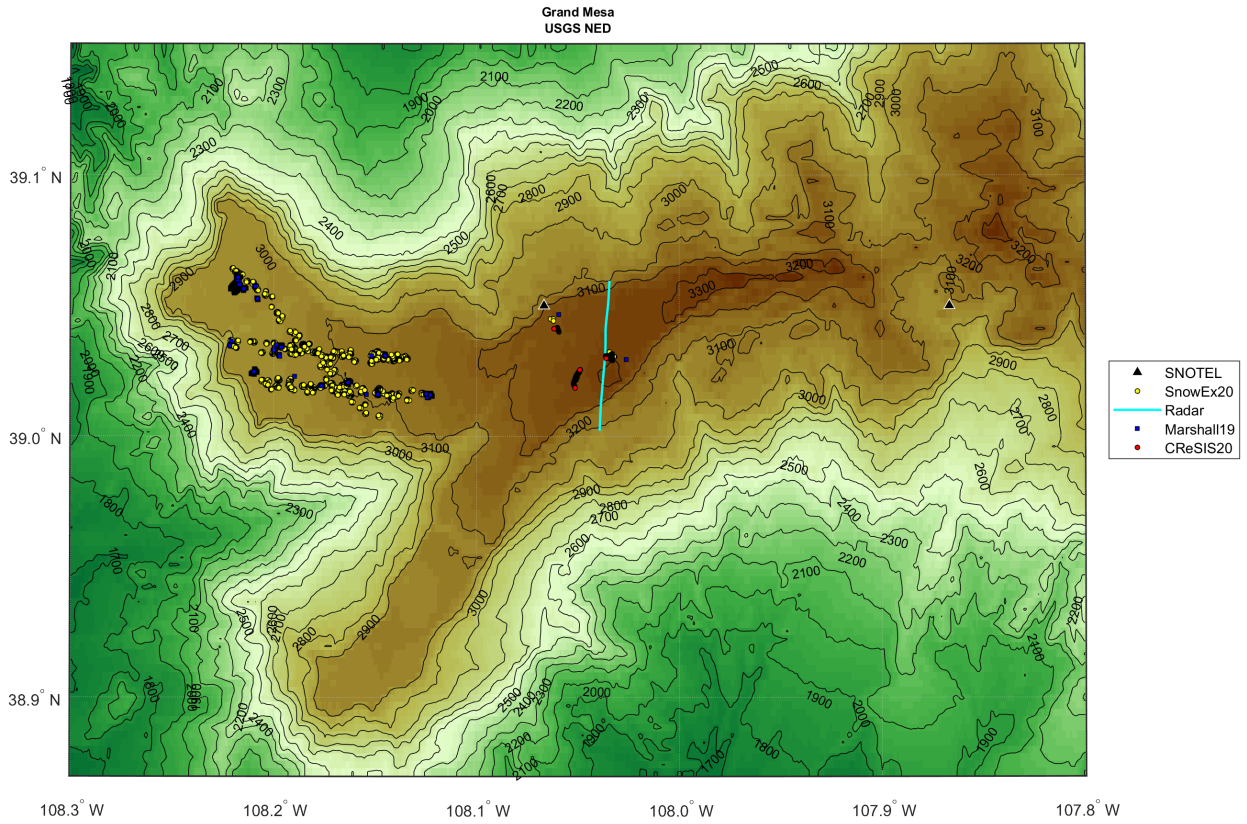

Figure 3.1: Map of Grand Mesa with elevation data from the USGS National Elevation Dataset (NED). Elevation is contoured every 100 m. The locations of SNOTEL stations (black triangles) and snow depth measurements for each dataset is marked: Marshall 2019 (blue squares), 2020 SnowEx (yellow dots), and 2020 CReSIS (red dots). A segment of the flightline used in the analysis is also plotted (cyan line).

Grand Mesa, CO from Jan 28 - Jan 31, 2020, to coincide with Snow Radar surveys (hereafter referred to CReSIS20). The snow depths were measured using avalanche poles like in Figure 2.1, and the latitude, longitude, and elevation measurements were from a handheld GPS receiver. Additional snow depth measurements from NASA 2020 SnowEx (Hiemstra et al., 2020) (hereafter referred to as SnowEx20) are used to supplement the study which occurred from late-January to mid-February 2020. The SnowEx20 measurements obtained snow depth measurements using magnaprobe and mesa2 instruments that can also automatically create GPS logs. Snow depths were measured in a spiral starting from a central snow pit location. A measurement was taken every 3 - 5 meters along a spiral track and final spirals averaged anywhere between 50 to 100 m. Furthermore, 2019 measurements from HP Marshall (hereafter referred to as Marshall19) are used, where snow

depths were measured from March 25 to March 29 using the automated probes. Flight surveys were taken using the FM-CW snow radars during this time period. In order to limit differences in GPS instruments uncertainty, elevation values from the ASO Point Cloud Digital Terrain Model (PCDTM) (Painter et al., 2020) was used across all of these snow depth measurements (Figure 3.7c). The elevation measurements are at a resolution of 3 m and reflect the bare earth elevations excluding trees and snow cover.

3.1.1 Climatology

To understand the climatology and snow depth annual variability, measurements were used from two SNOTEL stations on Grand Mesa: Mesa Lakes (622) and Park Reservoir (682). From all available measurements from both sites (Table 3.1), the climatology of snow depths and snow water equivalent is provided. Mesa Lakes measurements were taken from 2006 to 2020 and Park Reservoir measurements were taken from 1997 to 2020. Quality control of data was applied following some of the methods used in Serreze et al. (1999) where negative values, missing values, and erroneous values greater than 5 standard deviations were flagged. These flagged values were then backfilled using an interpolation scheme. SWE was measured first since the early 80's, so a climatological mean from 1981 to 2020 is reported for SWE. The snow depths and SWE for 2019 and 2020 started off very similarly, but start to diverge starting mid-January. The 2019 snow depths were the deepest during February and March and also the deepest snow depths recorded at the Mesa Lakes station. Park Reservoir also tends to report deeper snowpack compared to Mesa Lakes later into the snow season.

The summary of in situ ground surveys from 2019 and 2020 are listed in Table 3.2. During March 2019, the snow depths were double than they were during January and February of 2020, with the average snow depth being almost 2 m compared to the average of 1 m snow depths in 2020. We observe that standard deviations from 2019 were also double compared to standard deviations from 2020 measurements, but when we account for the differences in the mean, standard deviations are comparable with measurements spanning approximately 15% of the mean. Also, we

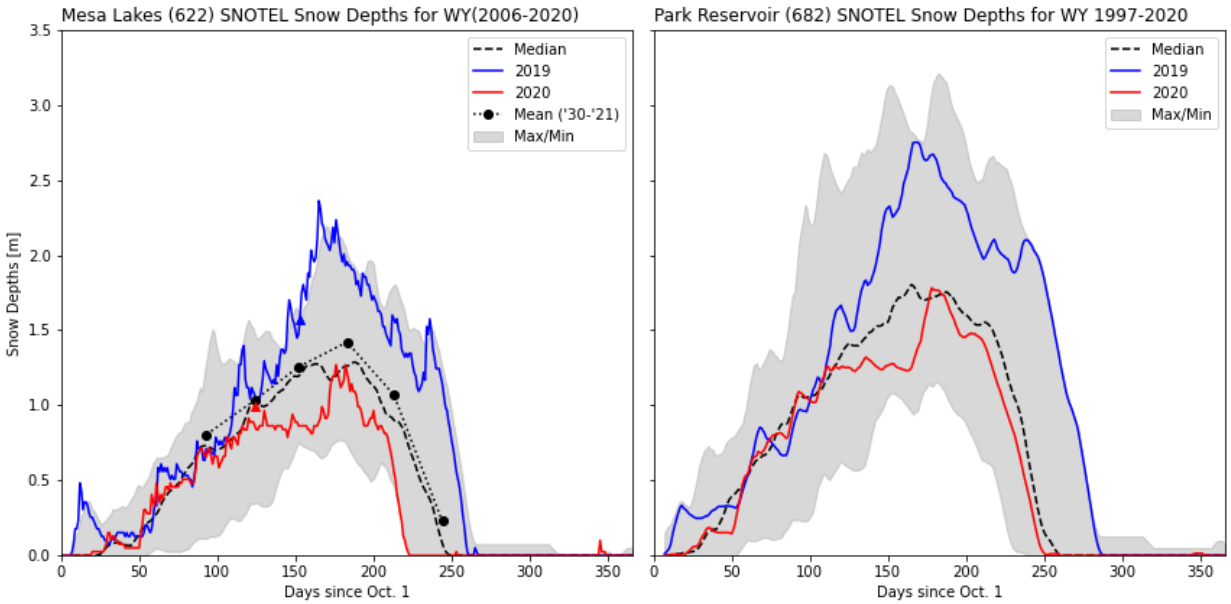

Figure 3.2: A rolling average of the median snow depths with a window of 7 days are plotted for Grand Mesa SNOTEL stations: Mesa Lakes (left) and Park Reservoir (right) for a water year (starting Oct 1 to Sep 30), and showing maximum and minimum (shaded areas) snow depths from the times of measurements. Average snow course measurements (Mean ('30-'21)) for snow depths at the beginning of the month are shown (black dots and dashed lines) along with snow course measurements in March 2019 and February 2020. SNOTEL Snow depths for water years 2019 (blue line) and 2020 (red line) are plotted to show differences in snow depths.

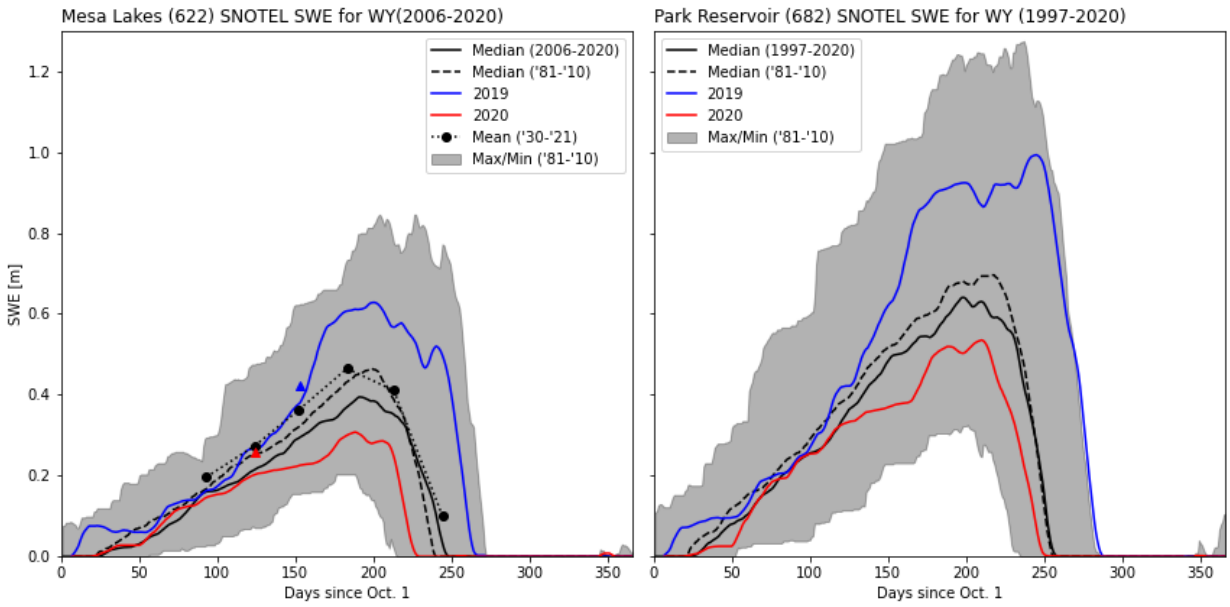

Figure 3.3: Similar to Figure 3.2 but dark grey shaded area shows the maximum and minimum SWE for a climatological period between 1981 to 2010. Two medians are also plotted for the climatological period (dashed black line) and an observational period (solid black line) where SNOTEL measured both snow depths and SWE.

must note the higher magnitude of individual measurements from the SnowEx20 dataset compared to both the CReSIS20 and Marshall19 datasets by several orders of magnitude. To put these in situ measurements in context, the monthly averaged snow depths from SNOTEL and snow course (SC) measurements are provided on Table 3.3. We see similar trends of deeper snow depths in the 2019 season compared to the 2020 season across both Mesa Lakes and Parks Reservoir stations.

Table 3.1: Summary of available measurements for the Mesa Lakes and Park Reservoir SNOTEL Stations as available from the USDA portal. 4 values are reported for air temperature: Observed, Maximum, Minimum, and Average. The Park Reservoir station also collects soil moisture and soil temperature data at depths of 2 in, 8 in, and 20 in below the surface, whereas the Mesa Lakes station does not.

Report Type	**Units**	**Mesa Lakes**	**Park Reservoir**
Precipitation, Accumulated	in	Daily, Hourly	Daily, Hourly
Snow Depth	in	Daily, Hourly	Daily, Hourly
Snow Water Equivalent	in	Daily, Hourly	Daily, Hourly
Temperature	C	Daily, Hourly	Daily, Hourly
Soil Moisture/Temperature	%/C	N/A	Daily, Hourly

The Park Reservoir SNOTEL station also has deeper snow depths compared to the Mesa Lakes SNOTEL station. For the snow course measurements, surveys were conducted near the end of each month to represent values at the beginning of the next month. To clarify, the reported April 2019 measurements were actually conducted on March 28, which is why the April snow depth closely matches to the average Marshall19 snow depth. In 2020, the average snow depths for both SnowEx20 and CReSIS20 are larger than what the Mesa Lakes station reports. The February snow course measurements at Mesa Lakes has better agreement with the average snow depths from the in situ measurements. In order to quantify the bias and error between these two measurements, the data was averaged daily and compared against the daily SNOTEL snow depths. The mean bias error (MBE) and mean absolute error (MAE) are shown on Table 3.4. The SnowEx20 snow depth measurements differed only by 0.06 m (6 cm) to the Mesa Lakes SNOTEL measurements compared to the 0.20 m with the CReSIS20 measurements, mirroring the monthly differences between the two datasets. This is most likely explained by the more diverse conditions that SnowEx20 measurements were made in relation to the Mesa Lakes SNOTEL station's location, against the more open, and homogeneous conditions of the CReSIS20 measurements. For the 2019 measurements, we observe that the in situ Marshall19 measurements were larger by 0.16 m, but only have a bias error of 0.05 m (5 cm). The Park Reservoir measurements were consistently larger across all three in situ datasets.

Table 3.2: Summary Statistics for the Snow Depth Measurements for all ground surveys from 2019 and 2020

Dataset	**Mean (m)**	**Std. Dev. (m)**	**CoV**	**N**
SnowEx20	0.95	0.17	17.76%	37,904
CReSIS20	1.08	0.14	12.81%	484
Marshall19	1.97	0.32	16.26%	2626

Table 3.3: Summary Statistics for snow depths of SNOTEL stations (Mesa Lakes and Park Reservoir) and Snow Course Measurements for 2019 and 2020. All measurements are reported in m. SNOTEL snow depths are a monthly average, while snow course measurements represent the snow depths at the beginning of the month. Blank areas are where snow depths were not reported.

Data/Year	Jan	Feb	Mar	Apr
Mesa Lakes SNOTEL 2019	0.93	1.29	2.0	1.72
Mesa Lakes SC 2019		1.07	1.57	1.98
Park Reservoir SNOTEL 2019	1.33	1.94	2.59	2.24
Mesa Lakes SNOTEL 2020	0.75	0.87	1.0	0.9
Mesa Lakes SC 2020		0.99	0.97	
Park Reservoir SNOTEL 2020	1.17	1.27	1.49	1.48

Table 3.4: Error statistics between daily averaged in situ measurements and SNOTEL snow depths for Mesa Lakes and Park Reservoir. All measurements are reported in m.

	Mesa Lakes		Park Reservoir	
Data/Year	MAE	MBE	MAE	MBE
SnowEx20	0.067	-0.064	0.32	0.32
CReSIS20	0.20	-0.20	0.17	0.17
Marshall19	0.16	0.049	0.59	0.59

3.1.2 Comparisons with Radar Footprints

For each dataset, in situ measurements were clustered and aggregated into approximately 7 m x 70 m rectangles to simulate an FM-CW radar footprint. In situ measurements that were collected through transects like the Marshall19 (Figure 3.6a) and CReSIS20 measurements were split into discrete 70 m segments. In the case of the CReSIS20 measurements (Figure 3.6b), two snow depth measurements were taken approximately 3 m apart from a GPS waypoint to represent the 7 m spread of the radar footprint, which was then split into 70 m segments for aggregation. For the SnowEx20 data that was collected in spirals as in Figure 3.5, footprints were split into 7 m sections in the x-direction (longitude) spanning the entirety of the spiral. Any in situ clusters that contained less than 10 measurements were dropped from the analysis. Furthermore, in situ clusters were grouped into levels of 'High', 'Medium' and 'Low' representation intervals depending on the amount of coverage of the clusters' "footprint" as summarized on Table 3.5. The percentage used to rate the SnowEx20 clusters were calculated by first splitting the along-distance cluster to 5 m bins

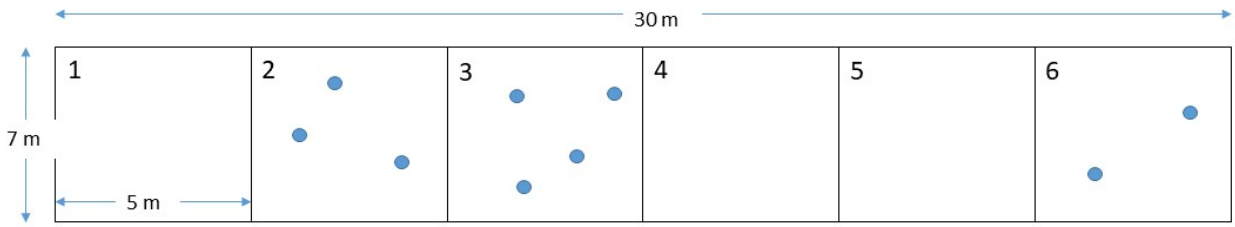

Figure 3.4: Example cluster of dimensions 7 m x 30 m split into 5 m segments with measurements (blue dots). Only 3 out of the 6 segments have measurements, so the effective length covered by the measurements of 15 m (3 segments $\times$ 5 m each) or 50%. This would be an example of a cluster with medium representation as of Table 3.5

Table 3.5: Representation levels for in situ clusters for the SnowEx20 Data based on percentages of the along-distance of a simulated radar footprint covered by in situ measurements. (i.e., an in situ cluster that covered 80% of a SnowEx20 site that was 100 m was labeled as a footprint with a high representation level

Representation Levels	Percent Covered Intervals
High	70 - 100%
Medium	40 - 70 %
Low	0-40 %

and counting the number of data points. The number of 5 m bins with data points were summed, multiplied by 5 and then divided by the total along-footprint distance. For example, if Pit A had an along-footprint distance of 100 m; it was split into 20 bins each 5 m long. If only 15 of these bins had measurements then, the percentage of cluster measured is calculated by $\frac{5m*15}{100m} = 0.75$ which will then binned as a cluster with high representation sampling. Representation levels were also set for the other 2 datasets. The CReSIS20 clusters were determined as high coverage due to the two snow depth transects across the entire 70 m along-footprint distance. The Marshall19 clusters also typically have good along-footprint coverage, but is deemed a medium coverage due to being a single transect. For each in situ cluster, the average and median snow depths were calculated. The standard deviation and the coefficient of variation (standard deviations expressed as a percentage of the mean) was also calculated for each cluster. The average elevation of the data cluster was also calculated.

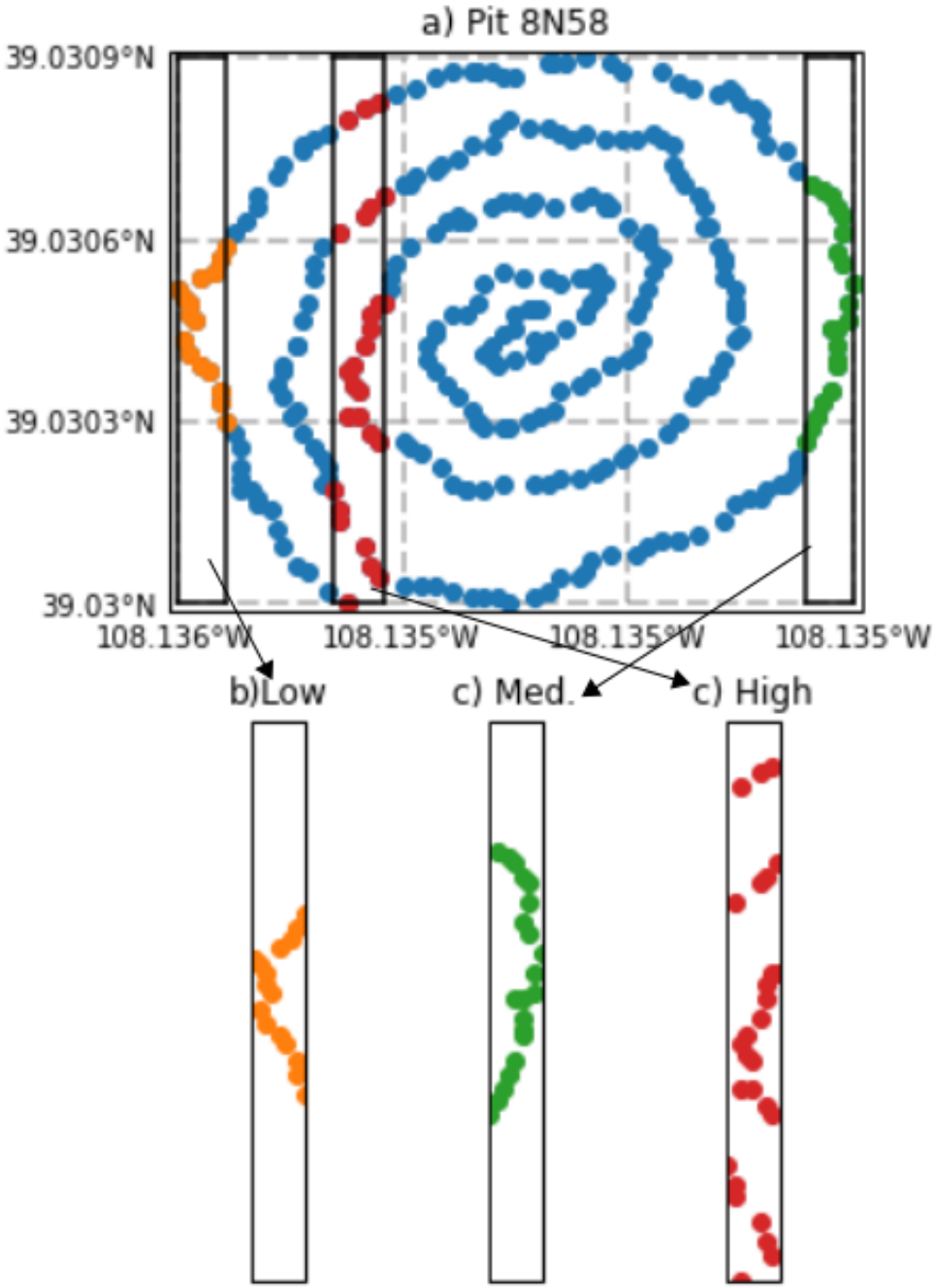

Figure 3.5: Clusters from an example SnowEx 2020 Spiral. The spiral was split into 7 m segments longitudinally, and using the maximum North-South distance of the spiral clusters. This examples shows clusters with Low (bottom left), Medium (bottom middle), High (bottom right) representation levels depending on the amount of coverage of the cluster (see Table 3.5). These clusters are an example of 25%, 50% and 90% coverage of the full cluster length.

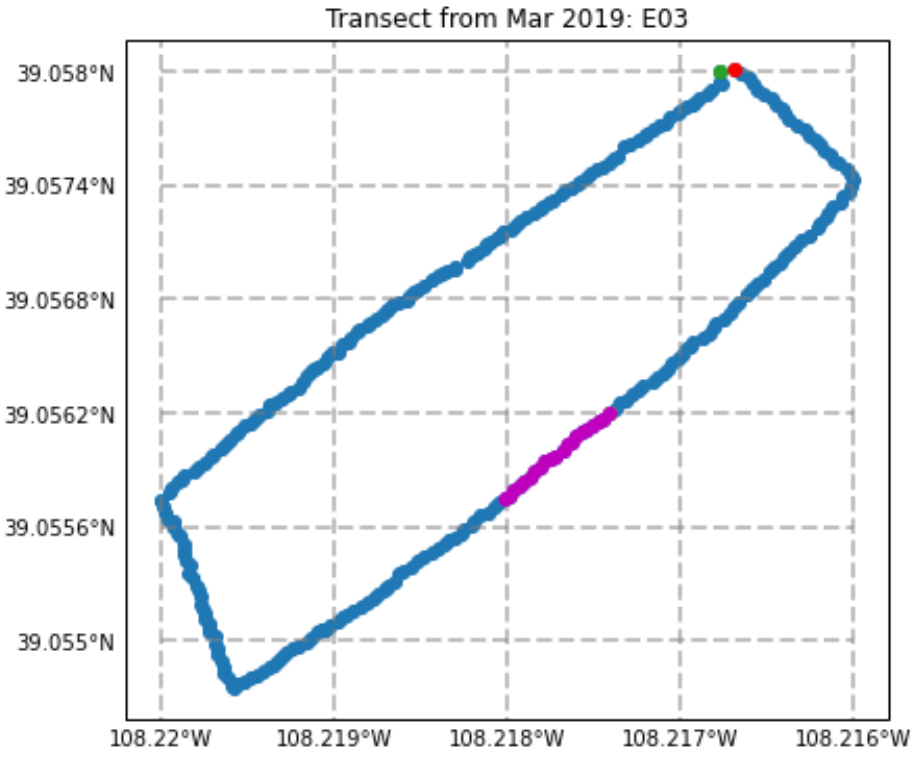

(a) Example Marshall19 Transect - Mar. 27, 2019

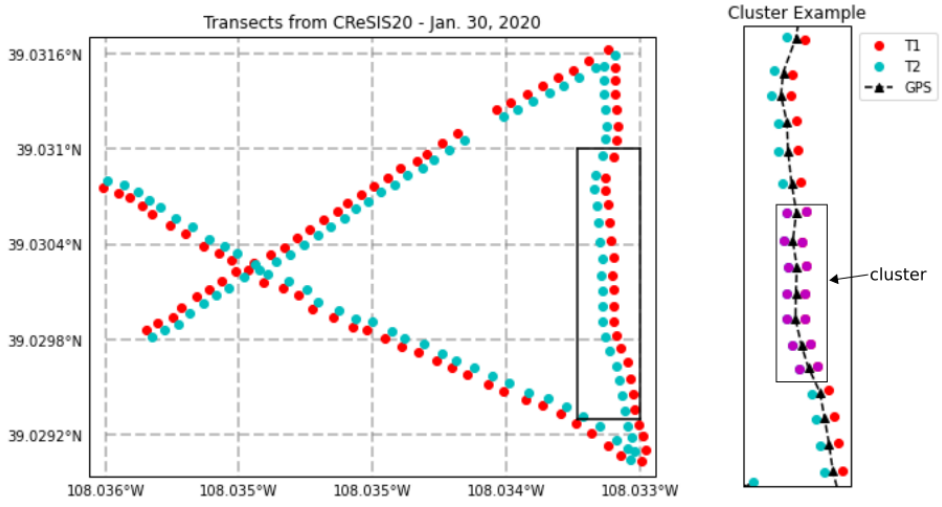

(b) Example CReSIS20 Transects - Jan. 30, 2020

Figure 3.6: Cluster creation for transects for a) 2019 and b) 2020. For 2019, the transect was split into approximately 70 m segments (magenta dots). Example of transect from 2020 CReSIS measurements on Jan. 30 showing the pairs of measurements for a GPS waypoint (bottom left). Zoomed in picture from figure on left. Magenta dots show in situ measurements clustered into $\sim$70 m segments.

In order to address the effects of vegetation on radar measurements and radar footprint uncertainty in Grand Mesa, 3 additional datasets of canopy height (Potapov et al., 2021), tree canopy cover (TCC) (Coulston et al., 2012), and land class (Jin et al., 2019) were used. Table 3.7 lists the parameters of the additional datasets of canopy height, tree canopy cover, and land class used in this study. The forest canopy height data from the Global Land Analysis and Discover team at the University of Maryland uses an integration of the Global Ecosystem Dynamics Investigation (GEDI) lidar measurements with Landsat data for 2019 (Figure 3.7a). The tree canopy cover and land class data are products of the new generation National Land Cover Database (NLCD) 2016 for the conterminous United States. The land cover (Figure 3.8) was categorized from Landsat imagery using an altered version of the Anderson classification (Jin et al., 2019). Table 3.6 lists and describes some of the relevant land cover types from the 2016 NLCD land cover data. For Grand Mesa, the top land cover classes were (52) Shrub/Scrub (30.2%), (42) Evergreen Forest (20.1%), and (41) Deciduous Forest (13.3%). The tree canopy cover is also derived from Landsat imagery where a 30 m cell is assigned a value between 0 to 100 percent representing the area or proportion of the cell that is covered (Figure 3.7b). It is assumed that all three datasets remain largely unchanged from 2016 to the present. Using the latitude and longitude of each snow depth measurements, the grid value for each dataset was extracted. The average canopy height and tree canopy cover was calculated for each data cluster, along with the mode of the land cover value was taken to primarily be the dominant land class value. For example, if out of 10 measurements 6 were made on a Evergreen Forest, 3 were made on an Mixed Forest, and 1 was made on a Developed area, the land cover for the footprint is determined to be an Evergreen Forest. To remove effects of tree cover that is covered by the snowpack, any canopy heights and tree canopy cover were flagged and equal to 0 if the canopy height was smaller compared to snow depths. For 2019 measurements, a similar filtering was done but for any canopy height 3 m or less and tree canopy cover was also reduced to 0.

Table 3.6: Table of the NLCD Land Cover Classes, Value, and classification descriptions from Jin et al. (2019).

Class	Value	Classification Description
11	Open Water	Areas of open water with less than 25% cover of vegetation or soil.
12	Perennial Ice/Snow	Areas covered by perennial cover of ice and/or snow greater than 25%.
21	Developed, Open Space	Areas with some mixtures of some constructed materials but mostly vegetation where impervious surfaces account for less than 20% of total cover.
22	Developed, Low Intensity	Areas of both constructed materials and vegetation with impervious surfaces accounting for 20-49% of total cover.
23	Developed, Medium Intensity	Mixed areas of constructed materials and vegetation where impervious surfaces make up 50-79% of total cover.
24	Developed, High Intensity	Highly developed areas where impervious surfaces make up 80-100% of total cover.
31	Barren Land	Barren areas of bedrock, scarps, sand dunes, etc. and vegetation account for less than 15% of total cover
41	Deciduous Forest	Tree dominated area of trees taller than 5 m and greater than 20% of total vegetation cover and 75% of trees shed foliage in response to seasonal change.
42	Evergreen Forest	Tree dominated areas of trees taller then 5 m and greater than 20% of total vegetation cover and more than 75% of trees maintain leaves all year.
43	Mixed Forest	Mixed forest areas where neither deciduous nor evergreen species make up 75% of total tree cover
52	Shrub/Scrub	Areas dominated by shrubs, typically less than 5 m tall, and shrub canopy makes 20% of total vegetation.
71	Grassland/Herbaceous	Areas where grammanoid and herbaceous vegetation make over 80% of total vegetation.
81	Pasture/Hay	Areas where vegetation (grass and/or legumes) greater than 20% of total vegetation is planted for grazing or for production at a perennial cycle.
82	Cultivated Crops	Areas used for production of annual crops or all lands actively tilled greater than 20% of total vegetation.
90	Woody Wetlands	Forest or shrubland areas with greater than 20% vegetation cover and periodically saturated or covered with water.
95	Emergent Herbaceous Wetlands	Areas of perennial herbaceous vegetation greater than 80% of vegetation cover and soul is periodically saturated or covered with water.

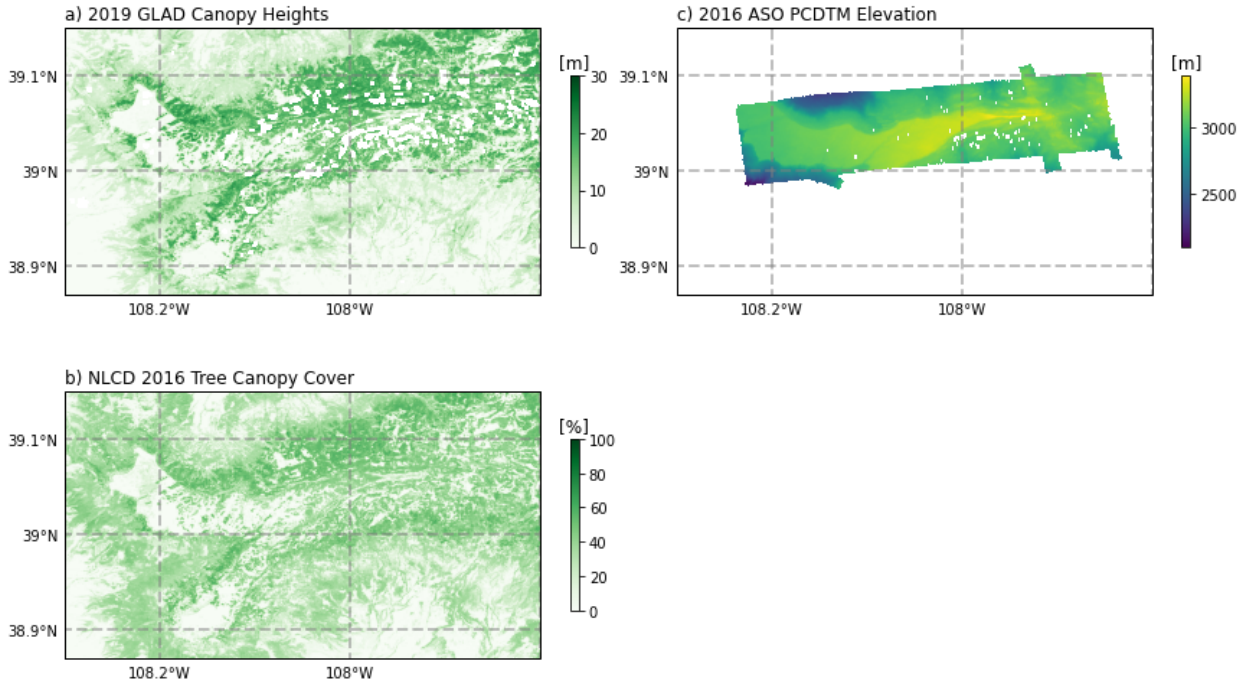

Figure 3.7: Maps of (a) canopy heights in m, (b) tree canopy cover as a percentage, and (c) elevations in m for Grand Mesa.

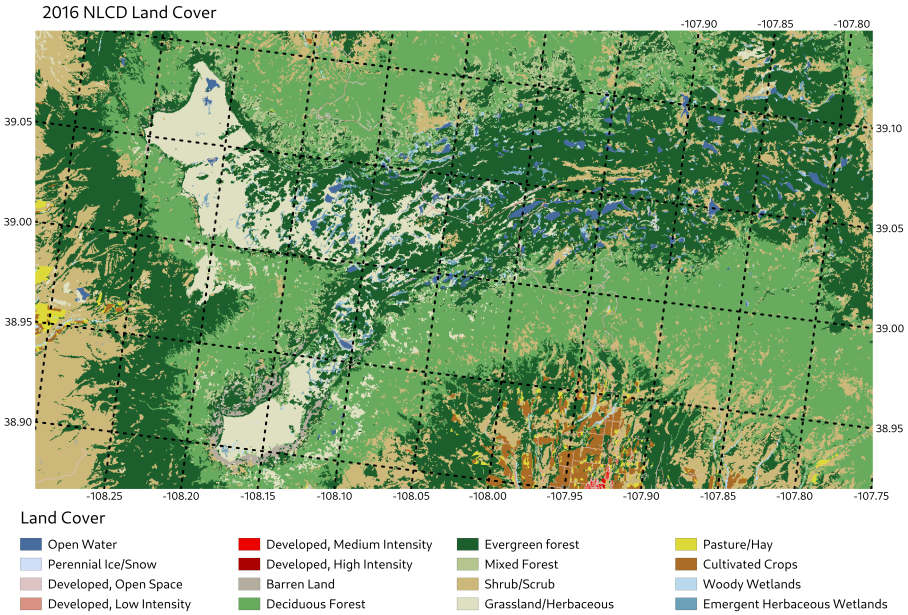

Figure 3.8: Map of 2016 Land Cover data for Grand Mesa.

Table 3.7: Parameters of the included forest canopy datasets

Data	Year	Units	Resolution	Source
Forest Canopy	2019	m	30m by 30m	Potapov et al. (2021)
Tree Canopy Cover	2016	%	30m by 30m	Coulston et al. (2012)
Land Class	2016	-	30m by 30m	Jin et al. (2019)

3.2 Echograms and Radar Data

Echograms and radar data were provided by the Remote Sensing Center at the University of Alabama. This study looks at a 6 km section of a flightline from January 30, 2020 at Grand Mesa. Figure 3.9 shows the full bandwidth echogram for the full flightline segment. The location of the North-South flightline is also shown as the cyan line on Figure 3.1. Additional maps are also provided on Figure 3.14 showing the flightline with respect to elevation and canopy data. This segment was in close proximity to our in situ snow depth measurements in the CReSIS 2020 survey made on the same day. Additionally, the flightline passes over a state highway (orange/red segment of flightline).

Estimates of snow depths along the flightline can be made from the echograms by finding the difference between the top (snow-air interface) and bottom (snow-ground interface) layers of the snowpack. In order to identify these features the following algorithm was implemented. First, the full echogram is initially split into several different segments. Each segment is then filtered using convolution by passing it through a sharpening filter and a smoothing filter. The filtered data matrix, v, is then standardized by each column, i, representing a vertical profile using the formula below.

$$v_s(:,i) = \frac{v(:,i) - min(v(:,i))}{max(v(:,i)) - min(v(:,i))} \tag{3.1}$$

The snow interfaces can be picked by analyzing the echo return columns as shown on Figure 3.11. The best layer locations for snow is assumed to be located where peaks are greater than the mean of a subset of echo returns greater than a power of 0.7 (Figure 3.12). The lowest return is first

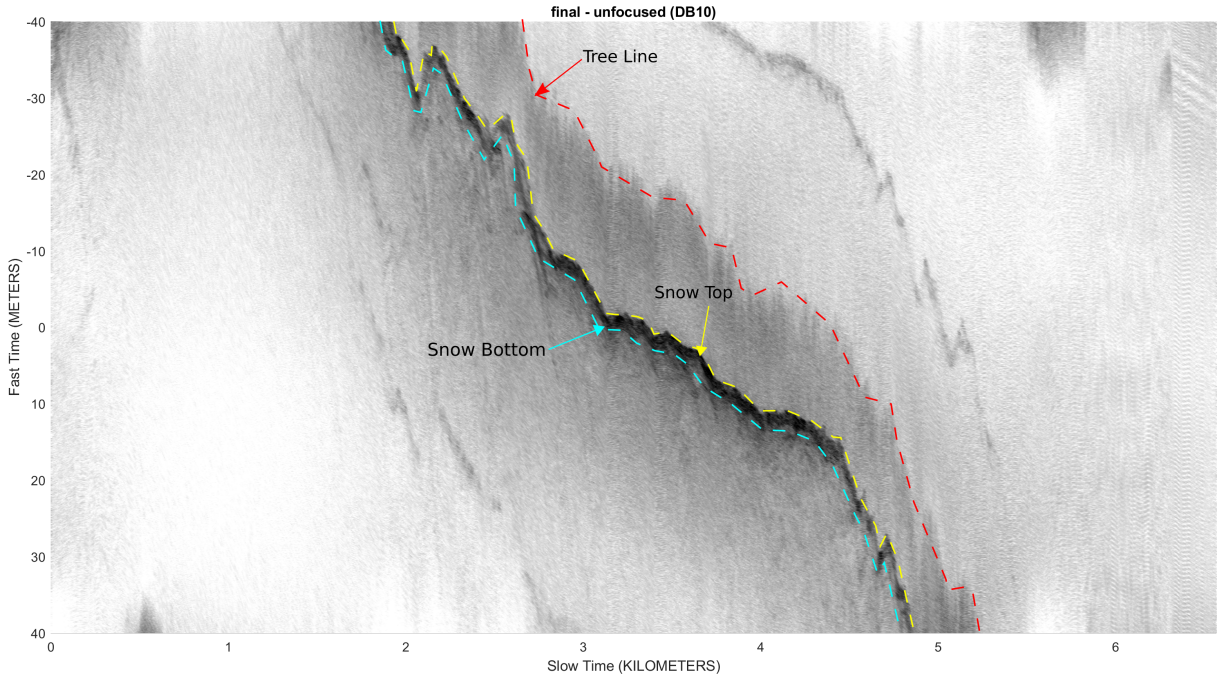

Figure 3.9: Full echogram of the Jan 30 flight segment, using the full bandwidth of the Snow Radar (2-16 GHz). The main features of the echogram are shown such as the Tree Line (red dashed line), as well as the snow top (yellow dashed line) and bottom (cyan dashed line) which are more defined using the full bandwidth.

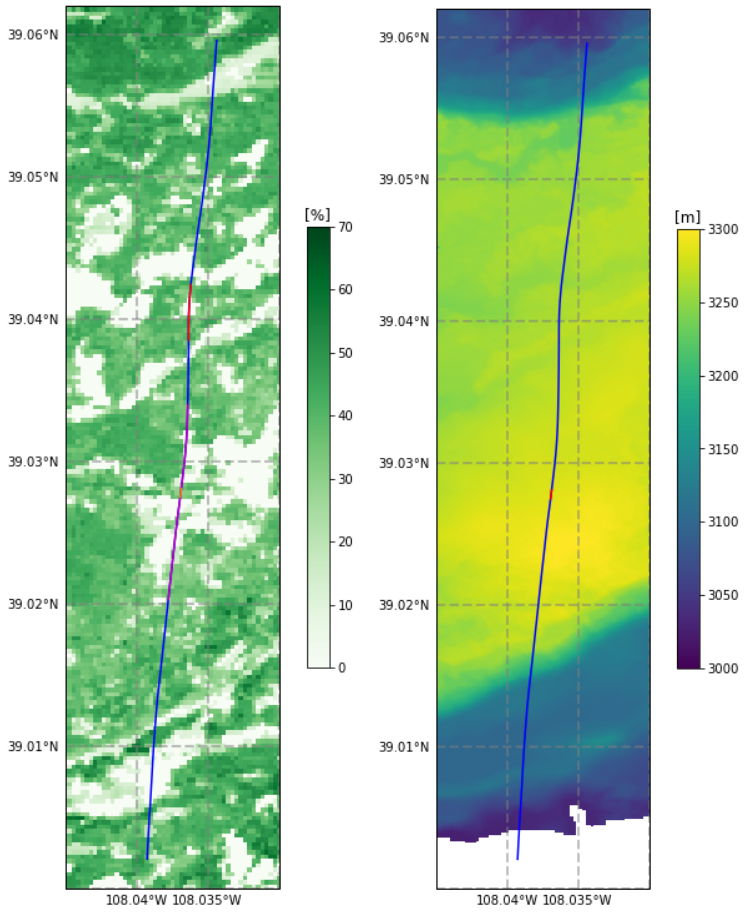

(a) TCC (b) Elevation

Figure 3.10: Maps of (a) tree canopy cover and (b) elevation with the flightline superimposed (blue line) on top. The orange segments near the middle of the flightline, represents the approximate locations of the road that crosses Grand Mesa.

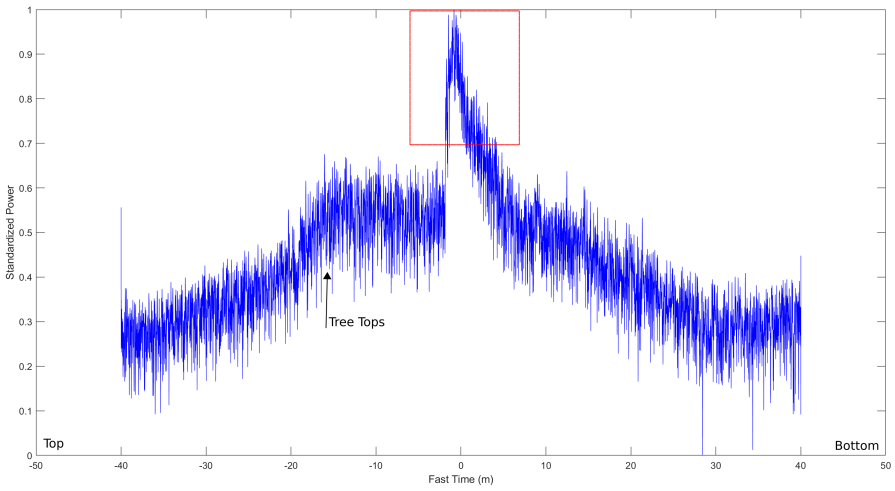

Figure 3.11: Example of a column of the normalized echogram power returns. We see a large peak towards the middle that shows the location where the snow layer starts. To the left of the peak, we see an increase in power that is due to the return signal from the tree tops.

chosen as the best guess of the snow/air interface or the top layer (filled green dot on Figure 3.12). The bottom layer is then chosen from a set of local maximums in the returns at a given distance away from the top layer. The distances were derived based on the average snow depth and standard deviations were based on the measurements closest to the flightline, which was the CReSIS20 data reported on Table 3.2 - 107.89 cm with a standard deviation of 13.82 cm. The shortest distance considered was 3 standard deviations below the mean - approximately 66 cm - and a maximum distance of 200 cm. While the lower bound for snow depths was set to the 3 standard deviations of the CReSIS20 measurements, the upper bound was chosen to reflect the maximum snow depths measurements obtained. The top 4 strongest returns were taken as the best guesses, wherever possible (filled red dots on Figure 3.12). The average of these results were taken as the best guess of the snow-ground interface or bottom layer of the snow. The snow depth is calculated as the height difference between the top layer and the bottom layer.

Out of the 6 km section, about 2.1 km of the flightline was picked as shown on Figure 3.13. These are denoted as Segment A and Segment B which are 0.5 and 1.6 km stretches in the echogram which contained the strongest returns. Two additional segments denoted Segment C and Segment D had returns which were likely affected by the physical environment. By comparing

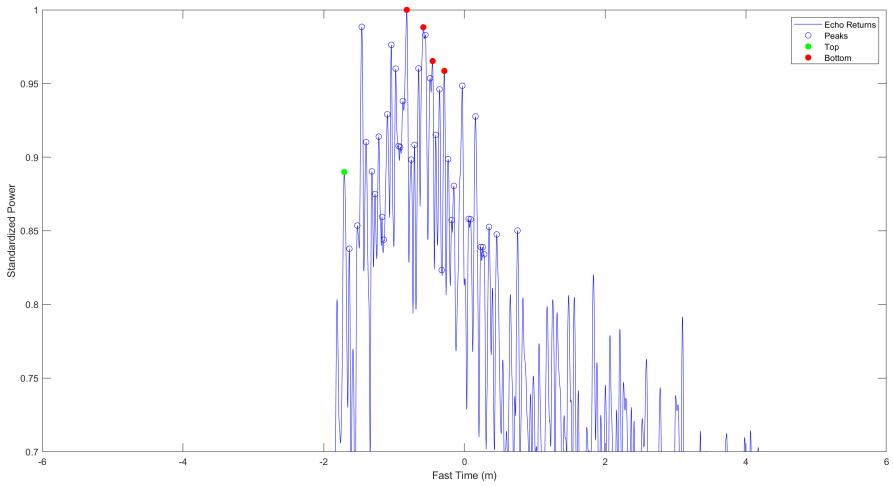

Figure 3.12: Zoomed in on red box of 3.11. Blue unfilled dots show peaks in the spectrum greater than the mean of all peaks above 0.7. The green filled dot, which is the leftmost point of this subset, is chosen as the best guess for the snow top layer. The red dots are possible locations of the snow bottom layer, that is searched from local maximums between 66 cm and 200 cm from the top.

picked results at different locations along the flightline, we can also look at how physical variability in changes to the landscape such as elevation, slope/aspect, and/or changes in the canopy can affect the accuracy in picking out the top and bottom of the snowpack. The tree canopy cover dataset described in Section 3.1.2 is used along with ASO DTM Elevation map. Subsequently, the slope, aspect and roughness are also used and calculated from the ASO elevation data using built-in operations in GDAL/OGR. The slope is measured in degrees and is the angle of inclination to the horizontal. Aspect is presented as a value between 0 to 360 which represents the azimuthal direction which the slope faces. Finally, surface irregularities are shown between two values: roughness and the terrain ruggedness index (TRI). Both TRI and roughness are similar measurements of surface irregularities but roughness is the greatest difference between a central pixel and its surrounding pixel and the TRI is the mean difference. There is sufficient variability in the segment in each variables to look at correlations.

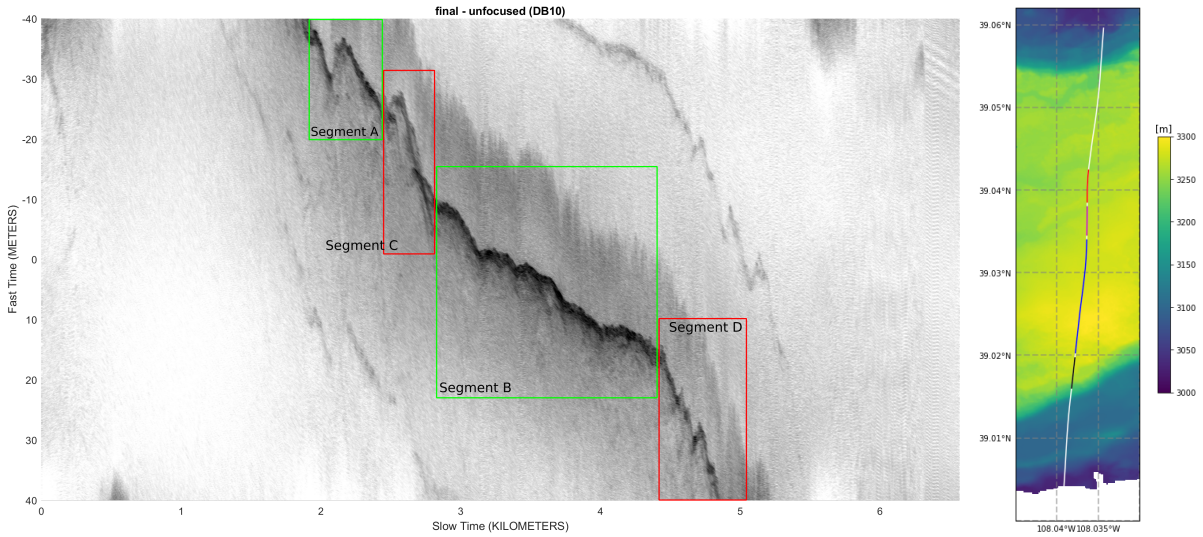

(a) (b)

Figure 3.13: a) Similar to Figure 3.9 but with red and green boxes to delineate locations of each segment. (b) Map of the flightline (white line) and elevation showing segment locations: Segment A (red line), Segment C (magenta line), Segment B (blue line) and Segment D (black line).

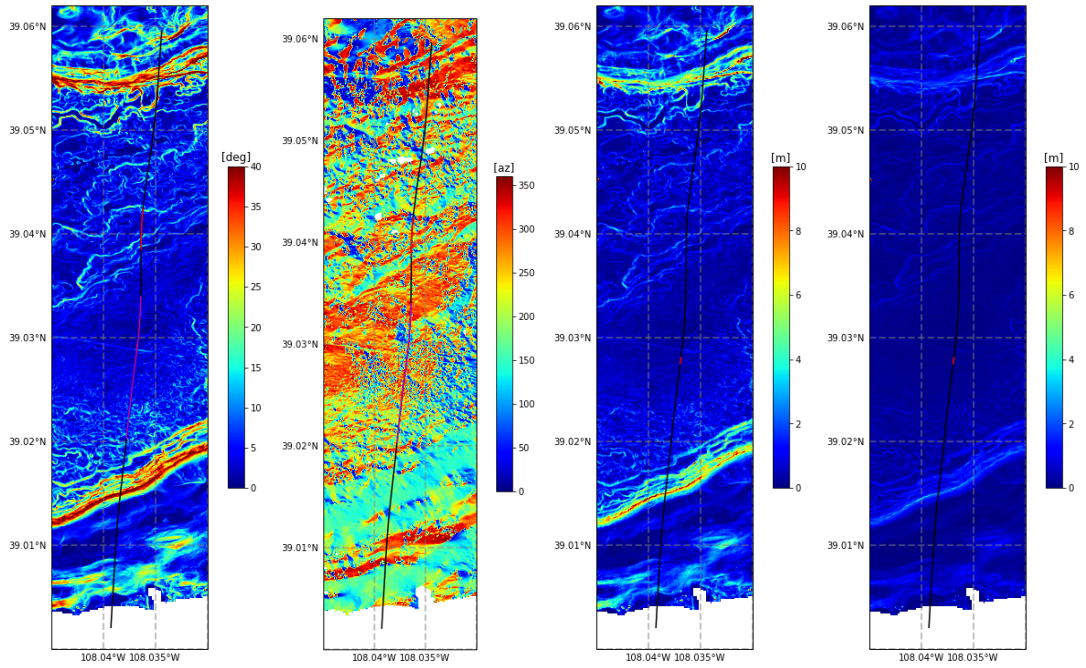

(a) Slope (b) Aspect (c) Roughness (d) TRI

Figure 3.14: Maps of (a) slope, (b) aspect, (c) roughness, and (d) TRI which were calculated from the ASO 3m DTM elevation data. The flightline (black line) is also superimposed on top.

Table 3.8: Variables used for the regression models

Var	Units
year	-
month	-
canopy height	m
elevation	m
tree canopy cover	%
land cover class	-

3.3 Regression Analysis

After examination of snow depth variability within a radar footprint, a linear model was used to predict the snow depths for given conditions for comparisons. A multi-linear model regression was fit using the in situ data. A linear regression model such as the following:

$$\hat{y} = b_0 + b_1 \cdot x_0 + ... + \varepsilon \tag{3.2}$$

where the predicted value ($\hat{y}$) is fit to a linear equation using coefficients (b_i) for data (x_i) for any number of i variables. The list of variables or features used to fit the linear models are summarised on Table 3.8. Along with the least squares regression, a recursive feature elimination scheme with cross validation (RFECV) in the python Scikit-learn package is also used to prevent overfitting and rank the features of the regression model. While fitting a linear model, fitting multiple features can lead to creating a perfectly fit line over data. Recursive feature selection or elimination schemes helps to not oversimplify a model with too little significant features and not have an overly complex model with redundant or non-important features leading to trained model with the minimally required number of features with reasonable accuracy in its predictions. Cross-validation schemes helps to evaluate and estimate the skill or accuracy of a model with limited data, by checking against subsets on data that it was not trained on. For a k-fold cross validation test, the dataset is split into k groups or folds. For each unique fold, that individual fold is reserved as the test, and the rest of the groups are used as the training set. In this study, a 10 K-fold was used as the cross-validation scheme.

Outside of just linear regressions, regressions using decision trees have also been shown to be fairly robust and also provides internal estimates to measure feature or variable importance. Using the linear regression model as a base of comparison, a regression model using the random forest (RF) machine learning algorithm like the one described by Breiman (2001) is compared and tested to see if estimates can be made for a given location on Grand Mesa to aid in snow depth estimates for radar processing. Regression models can also be formed using a binary tree, where the data is subdivided recursively. A dependent variable is split into partitions or branches based against a test with an independent variable or feature, where then each resulting branch is also split. Typically, singular decision trees can be prone to overfitting. The randomforest algorithm is an ensemble method based off of regression trees where multiple decision trees are created then regression results from the trees are aggregated, usually be taking the average of the output of various trees. Further randomness is added to each tree where a random subset of the features can be selected at a decision node where a dataset is split, reducing correlations in trees if certain features are a strong predictor of the dependent variable. The RF algorithms is argued to be robust to outliers and noise, and prevents overfitting. The RF regression algorithm was implemented using the Scikit-learn package in Python (Pedregosa et al., 2011).

The results using the ordinary linear regression and the RF regression will be compared to examine which method is better in obtaining snow depth estimates in Grand Mesa using the features listed on Table 3.8. Feature importance/ranking will be compared with both models to understand which environmental factors affects snow depths the most. The results between the least ordinary squares regression and randomforest regression will be compared by looking at accuracy scores, correlations between observations and predicted values, and error metrics such as the mean absolute error (MAE) and root mean squared errors (RMSE). Only the field surveys from 2019 and 2020 are used to create both models which will be the following datasets: SnowEx 2020, CReSIS 2020, and Marshall 2019. A 70/30 split is used for the training/testing data split.

Chapter 4

Results

This chapter presents the results of the analysis as outlined by Chapter 3. Section 1 discusses the results of the footprint analysis using the simulated clusters to establish the snow depth variability of a simulated radar footprint. Section 2 shows the results of the randomforest regression model. Finally, Section 3 shows the results of picking the Snow Radar data.

4.1 Footprint Analysis

A total of 1525 clusters were created across all of the 2020 snow depth (SD) transects and 90 clusters were created from the 2019 measurements. Figure 4.1 shows the 2019 and 2020 average cluster snow depths and internal standard deviations of the snow depth measurement shown as a percent of the mean. Despite larger snow depths in March 2019, the amount of snow depth variability in 2019 is smaller compared to 2020. When the internal snow depth variability between 5% and 95% percentiles are considered, snow depths vary between 2.5% to 18.6% for 2019 and between 5% and 26.1% in 2020. Despite lower snow depths in 2020, clusters showed higher variability with most measurements between 1 % to 30 % and a maximum of 51.4 %. Figure 4.2 shows a similar plot to Figure 4.1 but with the 2020 clusters only. The source of the highest snow depth variability in a cluster is from the 2020 SnowEx measurements. Both the clusters created from radar retrievals and our CReSIS measurements show similar levels of internal snow depth variability. When we group the data by month and year (Figure 4.3), we observe that in 2020 the changes to snow depth variability between January and February were small. However, all of the 2019 measurements were made in late-March, so a similar comparison cannot be made.

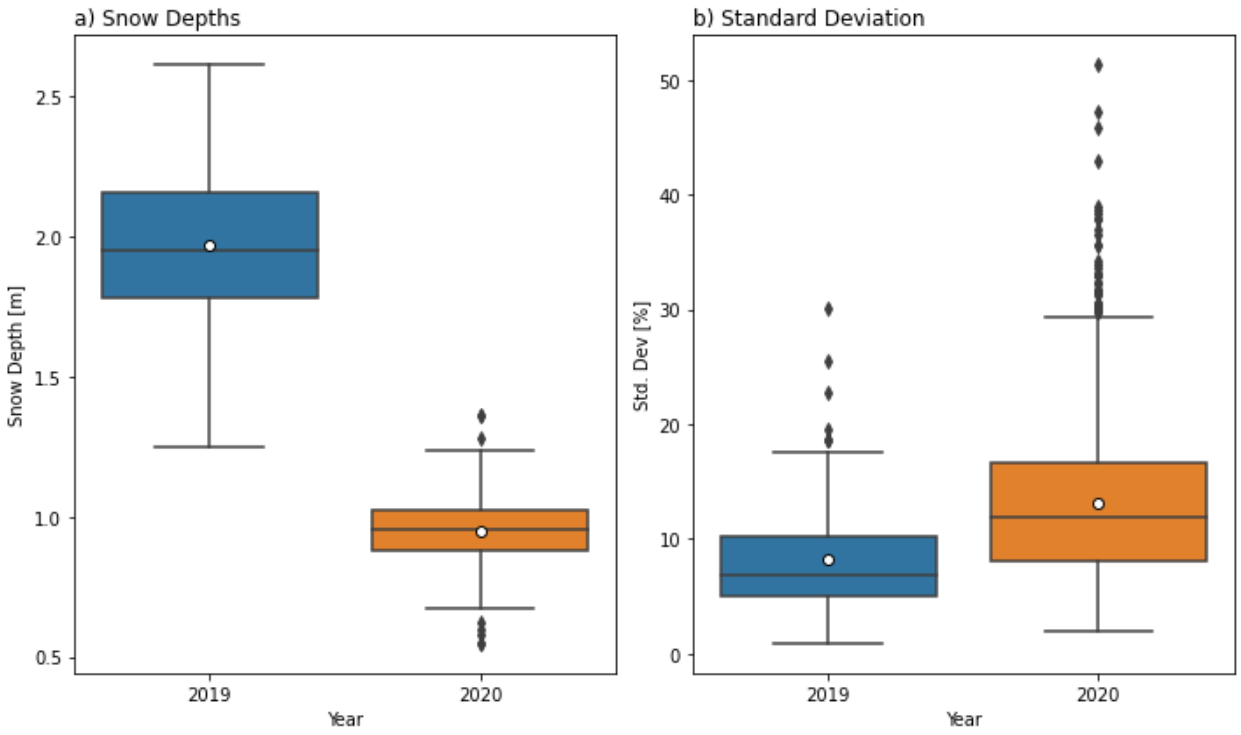

Figure 4.1: Boxplot of (a) average snow depths and (b) coefficient of variation for in situ clusters split by year.

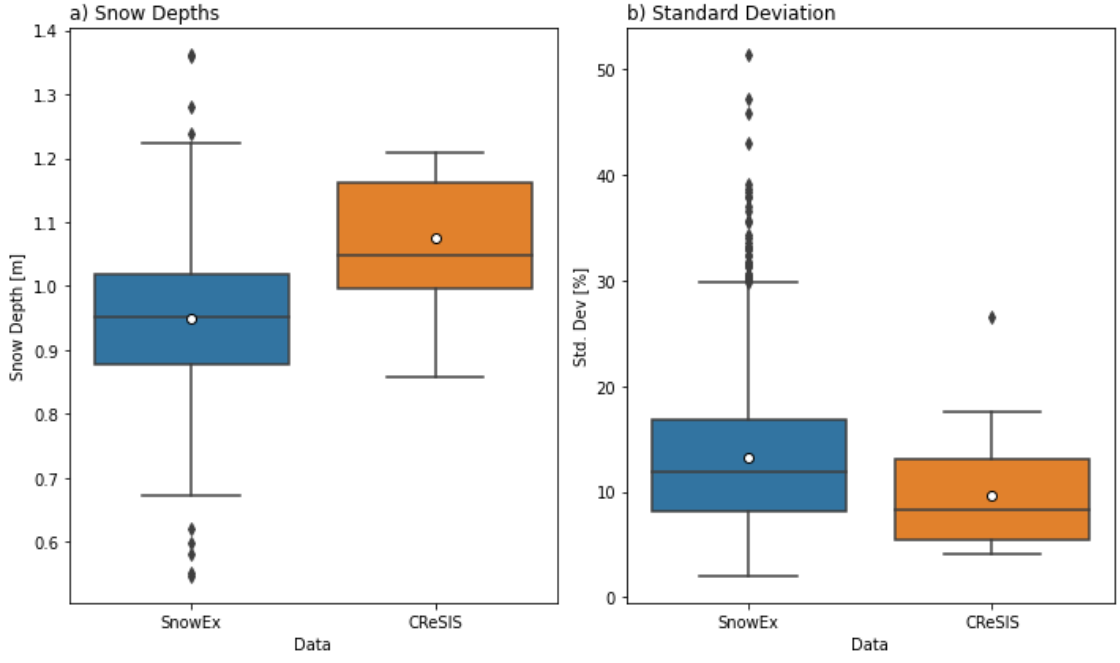

Figure 4.2: The same as Figure 4.1 but only for the 2020 simulated footprints.

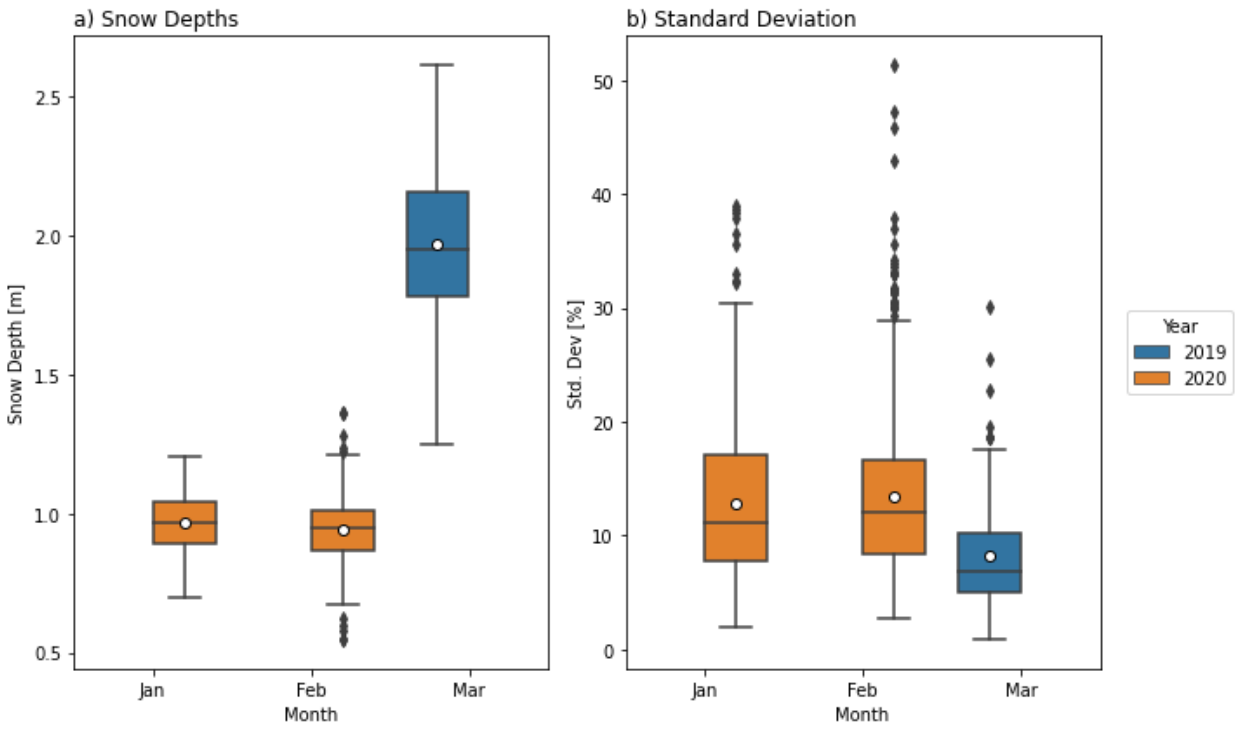

Figure 4.3: Boxplots grouped by month showing averages of in situ clusters a) snow depths and b) standard deviations.

Ignoring topological and physical parameters, we have found that in situ cluster parameters did not make any significant difference to the internal SD variability. We observed that internal snow depth variability does not change much as the number of measurements within an in situ cluster changes (Figure 4.4). The vast majority of in situ clusters had anywhere between 1 - 80 measurements for along-footprints distances of between 50-150 m, with the vast majority of clusters having between 10 to 40 measurements. The range of the number of measurements in a cluster was highest in the SnowEx20 spirals, where depending on measurements density within an expanding spiral, some clusters contained many more measurements. Due to different sampling rates, both the CReSIS20 and Marshall19 clusters had between 14 and 23 observations respectively, with similar levels of internal SD variability. At these scales near the radar footprint (70 m), approximately 10 seems to be the ideal lower bound for the number of measurements to provide anywhere between 5% to 30% of the mean SD of the cluster. Similarly, the along-side footprint lengths did not correlate with the internal SD variability. These lengths varied between 40 to 180 m, which are largely

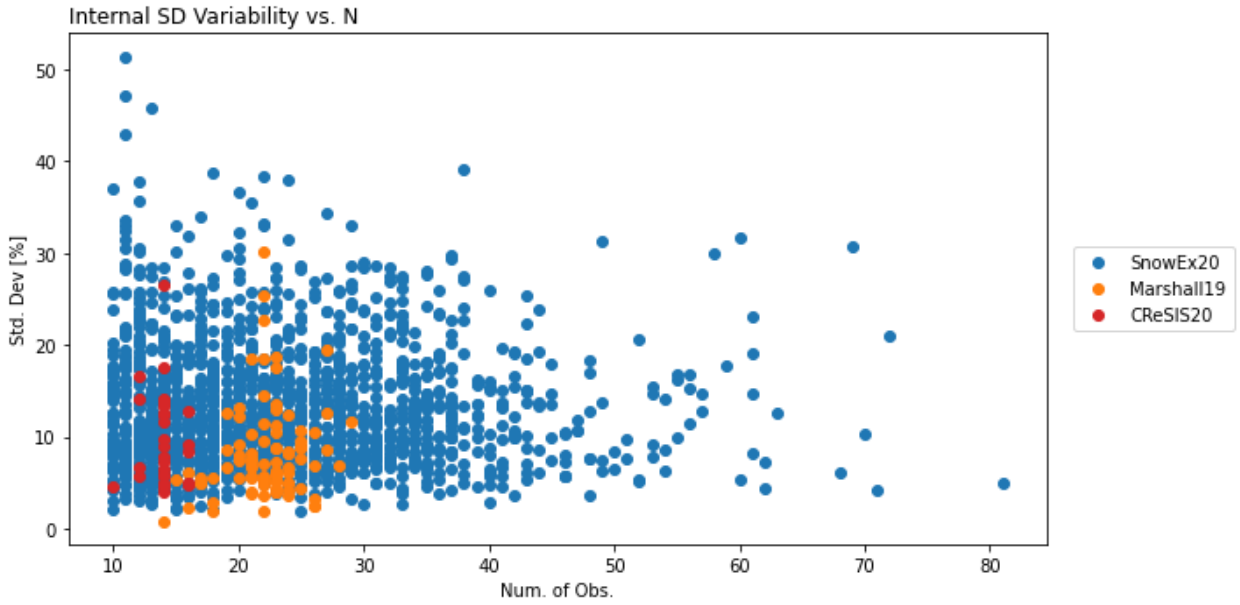

Figure 4.4: Plots of the internal snow depth standard deviations as a percentage of the mean against the number of observations within each in situ ground cluster.

the result of the various sizes of the SnowEx measurement spirals, with Marshall19 and CReSIS20 footprints mainly situated between 60 - 80 m. Correlation metrics suggest that the length of the cluster is generally uncorrelated with the footprint snow depth standard deviation (-0.057 across all three datasets). Figure 4.5 also shows how the footprint snow depth variability changes very little with the level of representation at the scales we are considering. Despite differences in maximum standard deviations, all three of the coverage representation levels are well within 10-15 % of the average snow depth, so snow depth variability is only largely a factor of the topological and physical parameters such as tree cover and not a result of this grouping.

To assess how physical variables like vegetation affect snow depths inside a simulated radar footprint, we compared the cluster statistics to vegetation measurements on Grand Mesa. Figure 4.6 shows a positive correlation between elevation and snow depths (r=0.528 and r=0.335 in 2019 and 2020 respectively), and a negative correlation between tree canopy cover and snow depths and between canopy height and snow depths. However, when we look at the relationships with snow depth variability (Figure 4.6), elevation is not correlated with SD variability, but both tree canopy cover and canopy heights are correlated with the standard deviations of snow depths inside

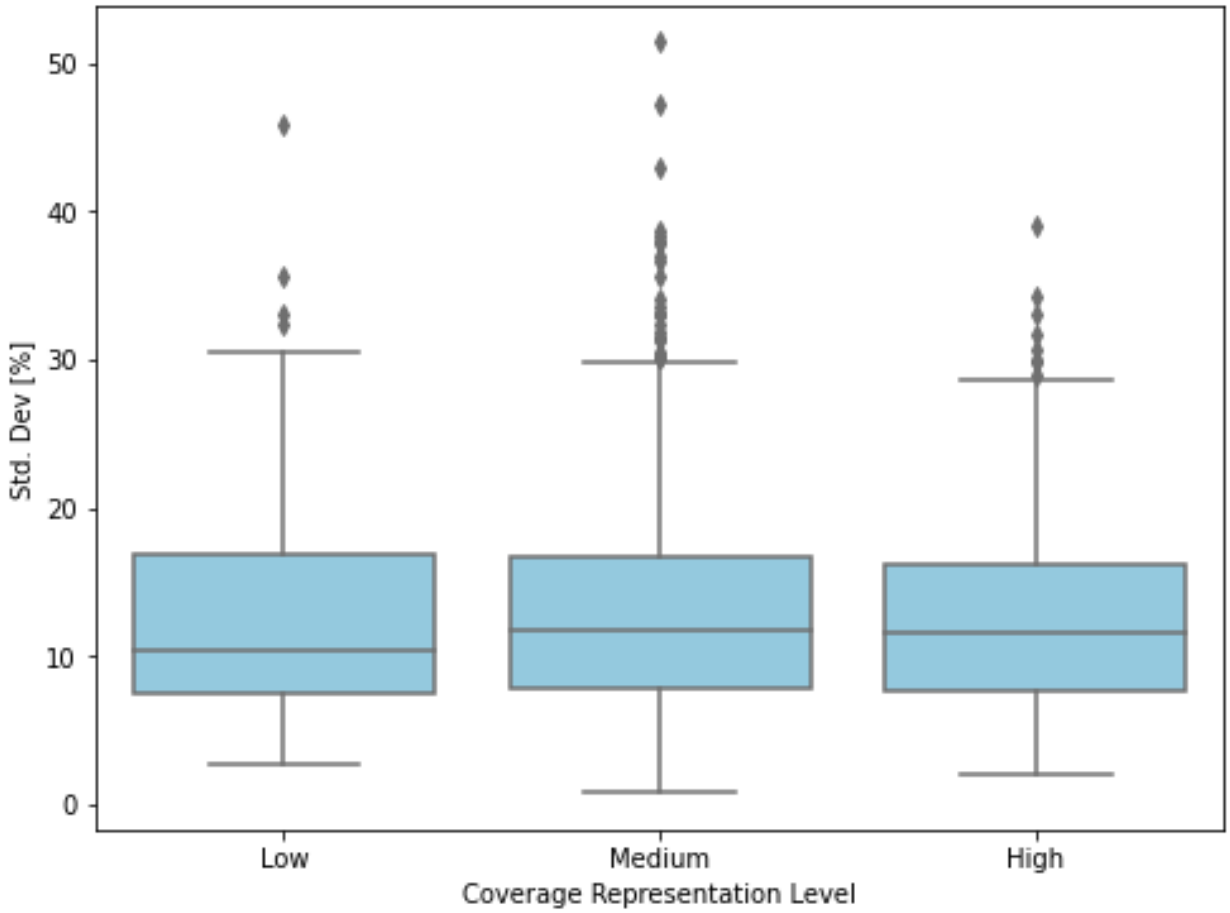

Figure 4.5: Boxplots of internal snow depth standard deviations of in situ clusters grouped by the level of the cluster sampled.

a simulated footprint. The discrepancy between the relationship between elevation against SD or SD standard deviations is strongly tied to the physical changes in elevation of Grand Mesa. Elevations on the Mesa tend to increase from west to east, which was also noted by Kim et al. (2017) in the SnowEx campaigns. Topography changes are likely to increase the average snow depths of closely clustered measurements, but since Grand Mesa is mostly flat, it is not likely to produce notable changes in variability of snow depth. The changes that vegetation brings as noted in Chapter 2, are likely causing both changes to snow depth and snow depth standard deviations within a simulated footprint. The reduction in snow depth that is caused by vegetation, will no doubt increase the variability of snow depths within approximately a 7 m by 70 m footprint.

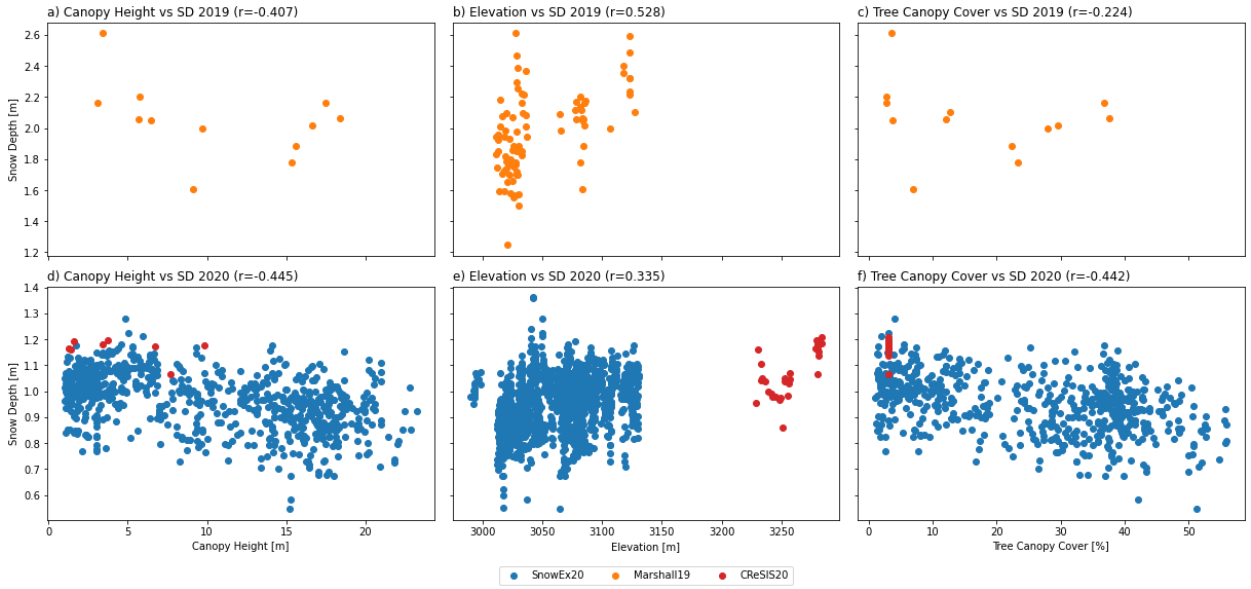

Figure 4.6: Scatter plots of (a, d) canopy height, (b, e) elevation, and (c, d) tree canopy cover against the average snow depth for the in situ clusters. Top row (a-c) are from 2019 and the bottom row (d-f) are from 2020.

In order to look at how different levels of tree canopy cover and canopy heights affect snow depths, the simulated footprints were classified into groups of similar forest structures. The classifications for the tree cover were done based on the SnowEx20 data, where measurements were grouped into 3 tree cover class from Treeless (0%), Sparse (1-30%), and Closed (>30%). The canopy height classifications were done based on the land class cover data. Any canopy heights below 1m in 2020 and 3m in 2019 were labeled as "bare ground" since they were most likely ei-

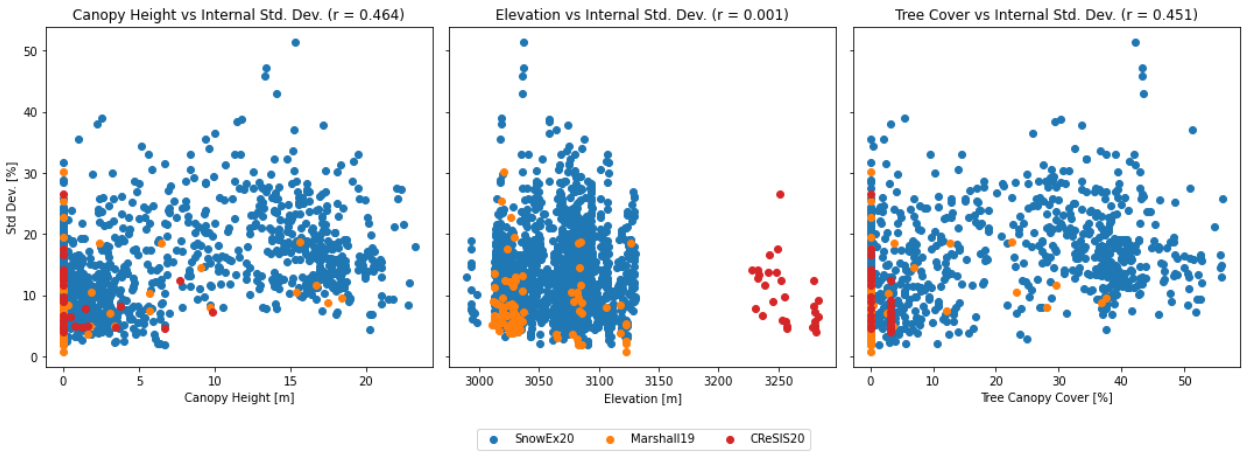

Figure 4.7: Scatter plots of (a) canopy height change, (b) elevation change, and (c) tree canopy cover change against the internal snow depth variability of in situ clusters.

Table 4.1: Number of in situ clusters that were grouped into 3 Tree Canopy Cover groups and 3 Canopy Height Groups.

	Tree Canopy Cover Groups		
Data	**Treeless (0%)**	**Sparse (1-30%)**	**Closed (> 30%)**
CReSIS20	19	12	0
SnowEx20	885	323	286
Marshall19	76	12	2
	Canopy Height Groups		
Data	**Bare Ground (0 m)**	**Middle (1-5 m)**	**High (> 5 m)**
CReSIS20	23	5	3
SnowEx20	729	288	477
Marshall19	78	3	10

ther covered completely by snow or had relatively no effect. Shrubby heights above the previously mentioned thresholds and less than 5m but above the snow were classified as "Middle" canopy heights, and anything greater than 5 meters was classified as having "High" canopy heights. Table 4.1 shows how many in situ clusters were classified into each group. To examine whether there are statistically significant differences between the groups for each dataset beyond a 5% confidence level, a difference of mean test was conducted summarized on Table 4.2.

These results are shown in Figure 4.8 for tree cover and Figure 4.9 for canopy height. We observe a consistent trend in canopy heights across all datasets. When we go from Treeless to sparsely covered clusters, a drop in snow depths in observed in all three datasets. The average

SnowEx20 clusters snow depths in Treeless regions was 0.04 m (4 cm) smaller to sparsely covered regions. Similar CReSIS20 and 2019 measurements were also 0.15 m (15 cm) and 0.12 m (12 cm) less than sparsely covered regions. However, only the SnowEx20 and CReSIS20 measurements were statistically significant. For all of the SnowEx20 measurements, the Covered regions had statistically significant less snow compared to the Treeless and Sparsely covered regions by 0.03 m and 0.07 m respectively. Differences in snow depths across the three tree canopy cover groups during the 2019 survey was not statistically significantly different from each other. When observing internal snow depth variabilities, we observed that Marshall19 and SnowEx20 measurements had less variability by 4% and 5% respectively, but the CReSIS20 variability increased by 5% when going from Treeless to sparsely covered regions. From Treeless to Covered regions, the SnowEx20 measurements observed smaller internal variability of 7.5 % and also smaller internal variability in Sparsely Covered regions compared to covered regions by 2.3 %. The 2019 field measurements found no levels of significant differences in internal snow depth variability between Treeless and Covered Regions, and Sparsely covered against covered regions.

When looking at canopy height groups, cluster average snow depths were not significantly different from each other across all three groups in the Marshall19 survey. Snow depth differences were statistically significant in SnowEx20 measurements, finding that bare snow and snow under trees of medium height had a difference of 0.08 m (8.4 cm) and snow under medium trees and tall trees had a difference of about 0.08 m (7.5 cm). For the CReSIS20 measurements, the only statistically significant difference in snow depths were under bare snow and medium height tree having a difference of 0.14 m (14 cm). Footprint snow variability was only different between bare ground and high canopy heights for Marshall19 by 4%, both bare ground and medium canopy heights had less internal variability in a cluster compare to high canopy heights for SnowEx20 Measurements by 7%, and the CReSIS20 had notable differences in cluster internal variability between bare ground and medium covered trees by 4%. The lack of measurements in more forested areas in the CReSIS20 and Marshall19 datasets (Table 4.1) makes it harder to establish clear trends in snow depths in the footprints. With tree canopy cover, the SnowEx20 data suggests that median

snow depth variability increased as tree canopy cover increased. However, the range of snow depths possible is also very high for each tree canopy cover class. This also suggests possibly the importance of wind and forest structures on snow accumulation as described in Currier & Lundquist (2018) which was not considered here because of a lack of wind data. A similar result is shown for canopy heights, with median snow depths in bare and exposed areas being similar to snow depths in tree covered areas with heights of about 5 m. The SnowEx20 data also shows that median snow depth variability seems to increase with increasing canopy heights (Blue violin plots on Figure 4.9). In both cases, snow depths was deeper under medium canopy heights (between 1 - 5 m) compared to both bare ground and high canopy heights (greater 5 m). A similar trend is shown in the Marshall19 surveys and the CReSIS20 survey, but since most of the difference of mean tests were not statistically significant, more measurements are needed whether this trend truly persists in forests on Grand Mesa. Snow depths are prone to change due to the effects of canopy, however there are also a variety of conditions that can affects snow depths in bare conditions as well such as wind, insolation, and topology.

Table 4.2: Results of Difference of Means test comparing whether these groups of tree canopy cover and canopy heights have statistically significant different means of snow depth and snow depth variability of simulated clusters with a student t-test at the 5% confidence level. The z-score is compared to the t test.

			Marshall19			SnowEx20			CReSIS20		
Snow Depth	Var 1	Var 2	$\Delta\mu$	z	t	$\Delta\mu$	z	t	$\Delta\mu$	z	t
	Treeless (0%)	Sparse (1-30%)	-0.123 m	1.514	2.201	-0.037 m	5.643	1.967	-0.149 m	8.168	2.201
	Treeless (0%)	Closed (> 30%)	-0.167 m	2.758	12.706	0.032 m	4.501	1.968			
	Sparse (1-30%)	Closed (>30%)	-0.044 m	0.484	12.706	0.069 m	8.143	1.968			
	Var 1	Var 2	$\Delta\mu$	z	t	$\Delta\mu$	z	t	$\Delta\mu$	z	t
	Bare Ground (0 m)	Middle (1-5 m)	-0.434 m	1.906	12.706	-0.084 m	14.377	1.968	-0.135 m	7.157	2.776
	Bare Ground (0 m)	High (> 5 m)	-0.028 m	0.442	2.262	-0.009 m	1.505	1.965	-0.094 m	2.334	4.303
	Middle (1-5 m)	High (> 5 m)	0.405 m	1.743	12.706	0.075 m	10.915	1.968	0.041 m	1.119	4.303
			Marshall19			SnowEx20			CReSIS20		
Internal Snow Depth Variability	Var 1	Var 2	$\Delta\mu$	z	t	$\Delta\mu$	z	t	$\Delta\mu$	z	t
	Treeless (0%)	Sparse (1-30%)	-3.9%	2.562	2.201	-5.1%	10.712	1.967	5.2%	3.621	2.201
	Treeless (0%)	Closed (> 30%)	-1.5%	2.165	12.706	-7.4%	16.397	1.968			
	Sparse (1-30%)	Closed (>30%)	2.4%	1.647	12.706	-2.3%	3.712	1.968			
	Var 1	Var 2	$\Delta\mu$	z	t	$\Delta\mu$	z	t	$\Delta\mu$	z	t
	Bare Ground (0 m)	Middle (1-5 m)	1.8%	1.438	12.706	-0.1%	0.256	1.968	4.5%	3.226	2.776
	Bare Ground (0 m)	High (> 5 m)	-4.0%	2.816	2.262	-7.5%	19.807	1.965	2.5%	0.962	4.303
	Middle (1-5 m)	High (> 5 m)	-5.8%	3.43	12.706	-7.4%	15.17	1.968	-2.0%	0.809	4.303

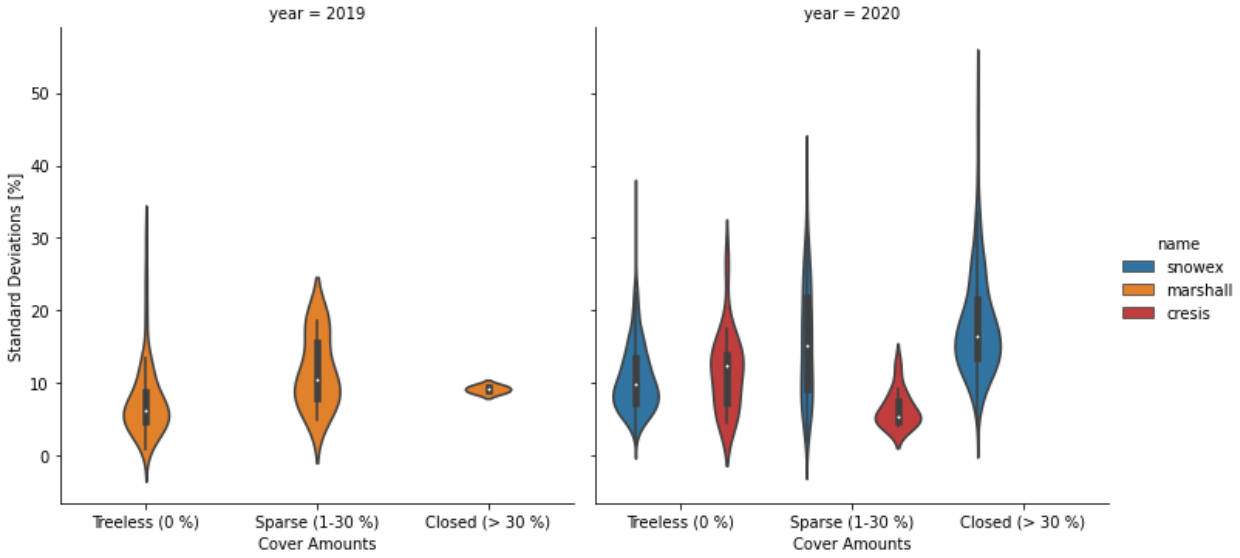

Figure 4.8: Violin plots showing both the distribution and a boxplot of the internal SD variability for each Tree Canopy Cover group for 2019 (left) and 2020 (right).

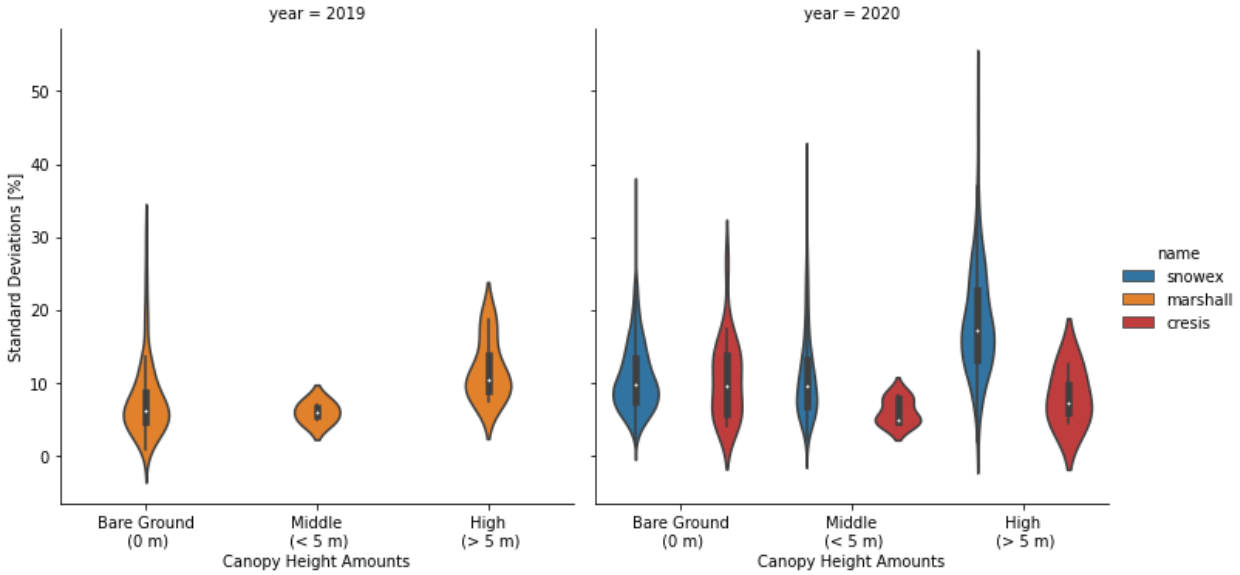

Figure 4.9: Similar to Figure 4.8 but for canopy heights.

Figure 4.10 shows the clusters' average snow depths grouped by the dominant Land Class. The land classes in order of frequency were Grassland/Herbaceous (1112), Evergreen Forest (413), Emergent Herbaceous Wetlands (79), Deciduous Forest (28), Mixed Forest (3), and Developed, Open Space (1). Out of all land classes, the snow depths were statistically different from each other except for the following pairs: deciduous/mixed forests ($\Delta\mu = 0.004$ m) and evergreen/mixed

forests ($\Delta\mu = 0.1$ m) in the SnowEx clusters, Grassland/Emergent Herbaceous Wetlands for the CReSIS clusters ($\Delta\mu = 0.07$ m), and Grasslands/Evergreen forests for the Marshall clusters ($\Delta\mu =$ 0.06 cm). Some differences in means were not able to be calculated where standard deviations were not available namely the Developed Open Space and Evergreen Forest classes for the CReSIS clusters. The aforementioned statistically insignificant pairs were results of small sample sizes of footprint land classes, or a comparison between a large sample size against a much smaller sample size often by 1 or 2 magnitudes. However, the largest snow depths appear to be coming from the Emergent Herbaceous Wetlands, with differences in mean snow depths between 0.06 - 0.18 m in 2020, and between 0.53-0.59 m in 2019.

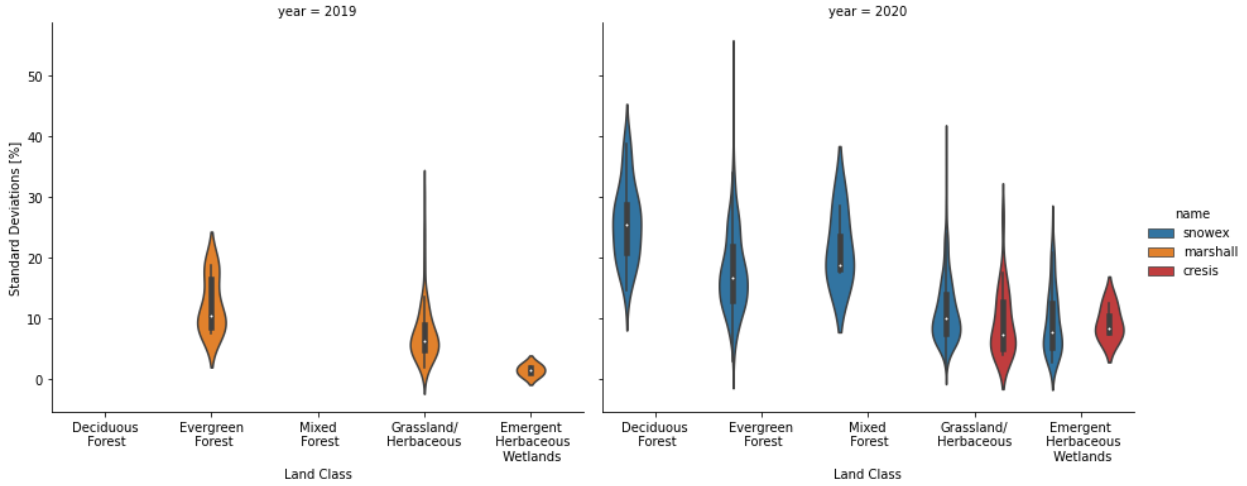

Figure 4.10: Violin plot showing the distribution and boxplots (grey box and white dot showing the median) of the internal snow depth variability split by the dominant land cover class of the in situ clusters for 2019 (right) and 2020 (left).

4.2 Regression Results

Regressions, especially randomforests, are highly affected by correlated variables which are shown on Figure 4.11. Like previously mentioned in Kim et al. (2017), elevations are highly correlated with longitude (0.925) in Grand Mesa, where elevations increases as we travel east. Another pair of highly correlated variables are canopy height and tree canopy cover with a correlation of 0.940. Both of these variables would be highly correlated as taller trees are more likely to be

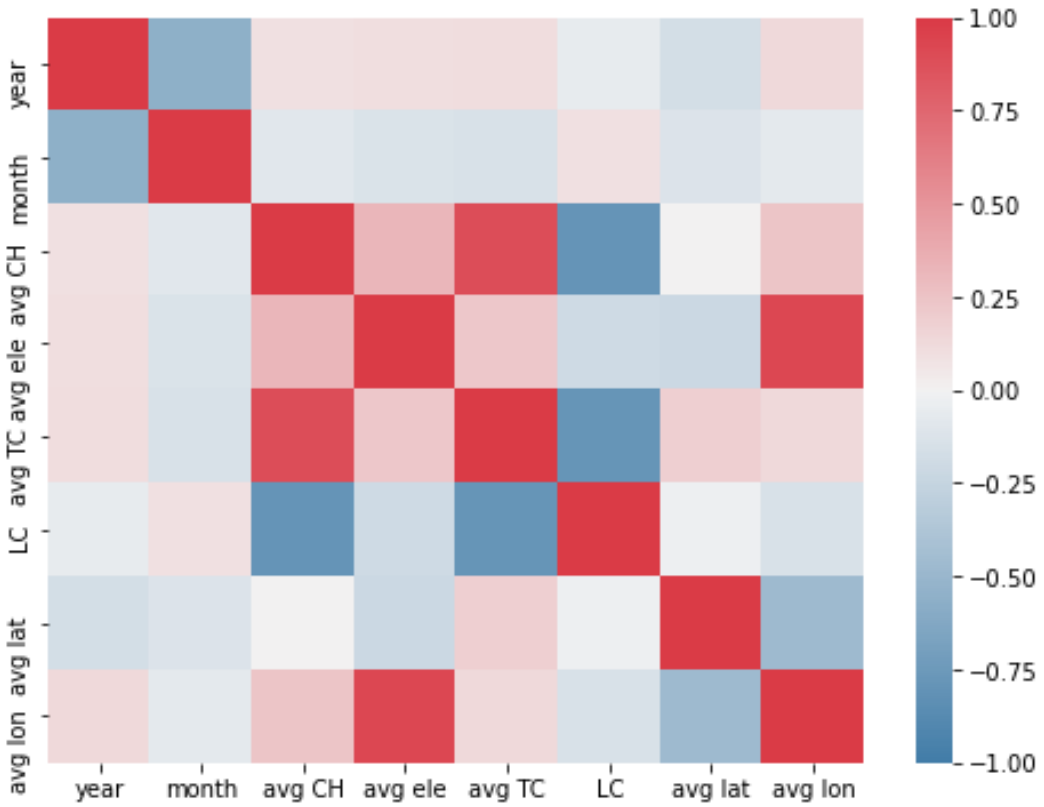

Figure 4.11: Correlation table for features to be used in the randomforest regressor. High correlations exists between elevation and longitude in Grand Mesa, along with high correlation between canopy height and tree canopy cover. The diagonal are correlations between a feature and itself and are perfectly correlated.

found in densely covered forests. Land cover was mostly anti-correlated with both canopy heights and TCC with correlations of -0.792 and -0.815 respectively. The strong anti-correlation can be explained by how the NLCD 2019 data classifies its land classes. Outside of developed areas and bodies of water, forested land classes are labeled with smaller numbers compared to non-forested land classes (refer back to Table 3.6). For example, the deciduous and mixed forest classes are labeled with values of 41 and 43 respectively while grasslands are labeled with a value of 71. Only bodies of water and developed areas are labeled in the data with values less than 40 (11 and 21-24 respectively), which are not very common on Grand Mesa. This creates the anti-correlated linear relationship where higher (lower) levels of canopy heights and TCC are labeled with a smaller (larger) land class value.

Before the regression was performed, a snow depth index (SNDI) was created for all of the

clusters' average snow depths to remove yearly variations in snow using the formula below.

$$SNDI_{20XX} = \frac{SD_c - \mu_{20XX}}{\sigma_{20XX}} \tag{4.1}$$

The average simulated footprint snow depth (SD_c) in 2020 will have a yearly averaged snow depth (μ_{2020}) removed and divided by the yearly averaged standard deviation (σ_{2020}). The Randomforest algorithm can also give insights into which variables are more important to the model with importance figures, measured as the mean decrease in impurity. Figure 4.12 shows the importance of each variable for the model simulations with the SNDI. The three most important variables were elevation (27%), canopy height (23%), and latitude (18%). Longitude and tree canopy cover had importance values of 16% and 12% respectively. Without the use of the SNDI, both the year and month were the two most important features with mean decreases in impurity by almost 35% and 46% respectively, since yearly variability in precipitation will limit the amount of accumulation. Removing yearly means through the SNDI, the month of measurement also had a slight impact, since snow depths will typically grow throughout the water year. Outside of temporal factors, location on Grand Mesa plays a large role in determining snow depths, with elevation being the leading feature of explaining snow depth variability. Land class cover does not seem to have much of an effect on the regression model, but with the correlation values, these values may be greatly diminished when fitted with both canopy height and tree canopy cover.

The results of the regression fit for the testing and training sets are shown on Figure 4.13. The randomforest model using the SNDI values had an out-of-bag (OOB) score of 0.672. Out-of-bag score is the accuracy of the model using only the trees for which the training set was omitted. The accuracy score for the testing set was 0.635. Figure 4.13 shows how the predicted snow depths performed compared to the actual values in the testing and training sets. Correlations between the observations and the predicted results were highly correlated in the testing set (0.797). The mean absolute error (MAE) was 0.261 and the root mean squared errors (RMSE) was 0.376, which corresponds to differences of about 0.04 m to 0.06 m in 2020 and 0.08 to 0.12 m in 2019. When

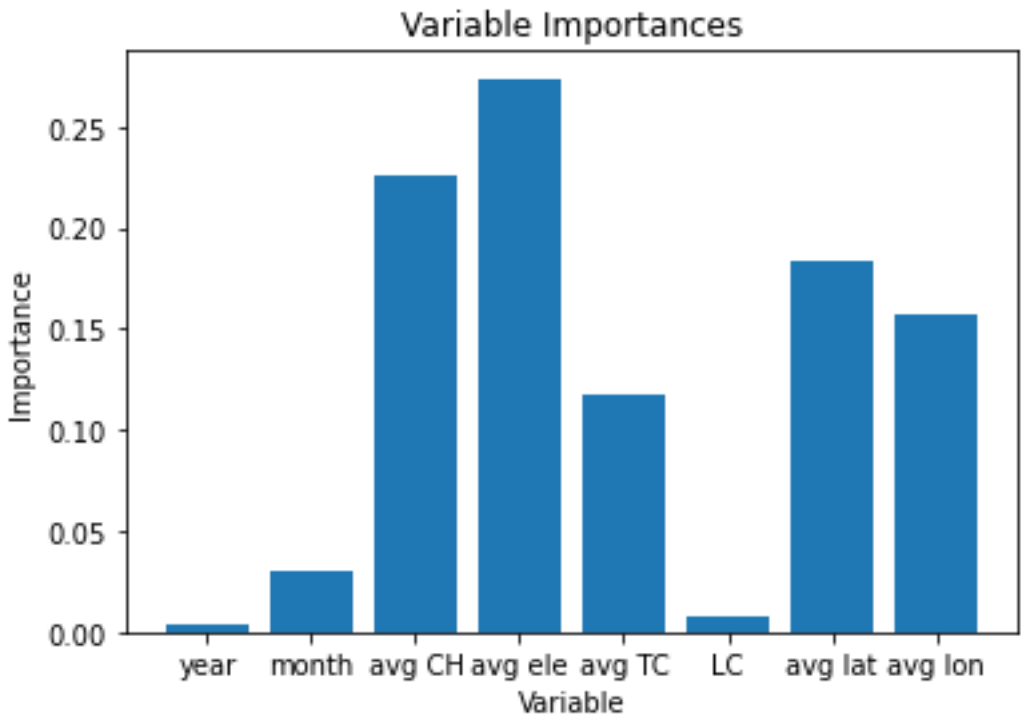

Figure 4.12: Bar plot showing each variable importance to the RF regression model. Feature importance is the percent decrease of the mean impurity.

fitting the model to regular snow depths, the OOB score performs better with a score of 0.931. The accuracy of the testing set only was 0.854. Without the yearly means removed, the MAE and RMSE was about 0.05 and 0.08 cm respectively. The difference between 2020 and 2019 are more clearly visible in this fitted model. Estimates for 2019 snow depths appear to be worse with the model tending to overpredict snow depths up to maximum of 0.69 m, likely due to the larger weight given to the 2020 measurements.

Results of the least squares regression with cross validations are shown on Figures 4.14 for detrended data. Comparing the results for the regular snow depths (not shown) shows that errors are higher using a least squares regression. The MAE and RMSE are 0.08 cm and 0.11 cm respectively, with an accuracy score of 0.797. While the results are linear as shown by the high Pearson correlations, the Spearman Rank Correlations are worse for the linear regression results (0.593 for LR and 0.854 for RF). This is also true for the detrended data. The linear regression was only able to achieve an accuracy score of 0.228 compared to 0.635 for the randomforest regression.

The MAE and RMSE was 0.414 and 0.546 respectively which an error of about 0.07 and 0.09 m in 2020 and 0.13 to 0.17 m in 2019. The linear regression model also did not select elevation as one of the more important variables with the detrended data. The linear regression result for the detrended data was also not as well correlated as the randomforest predictions.

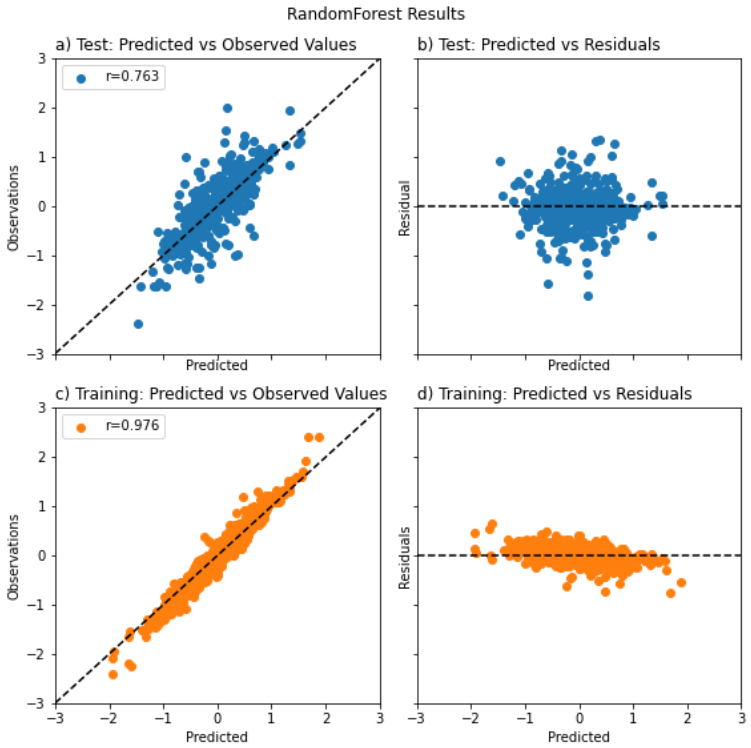

Figure 4.13: (a) Scatter plot of observed cluster snow depth indices against modeled snow depth indices of the testing data. Dashed black line of slope 1 to denote perfect correlations. (b) Scatter plot of predicted values against model residuals. The black dashed line denoting where residuals are equal to 0. (c) Same as (a) but for the training data. (d) Same as (b) but for the training data.

4.3 Results of Layer Picking

The results of picking snow tops and bottoms from segments A and B are shown on Figure 4.15 and 4.16 respectively and snow depth calculations are summarized on Table 4.3. Across 37 points in the .5 km section, the average snow depth for segment A was 1.15 m and the average uncertainty or standard deviation was approximately .21 m, or 18.2 % of the mean. Segment B had an average snow depth of 1.13 m and an average uncertainty of .20 m (17.3% of the mean) across 121 picked

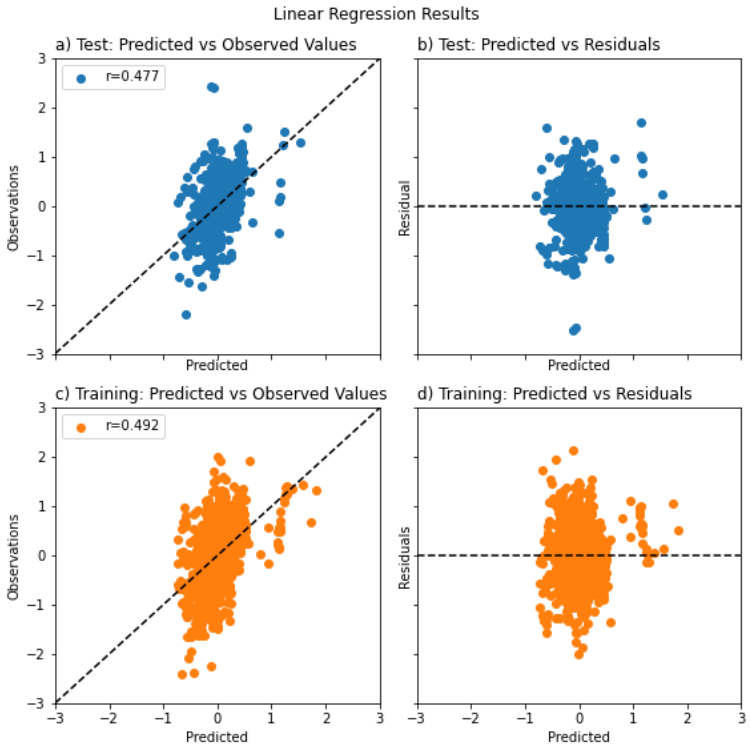

Figure 4.14: Similar to Figure 4.13 but for the linear regression model.

locations. Both segments had locations where a complete pick was not possible. On Segment B, the flightline passes over the main Grand Mesa Scenic Byway, which is made evident in the echogram by a strong line showing returns that are very distinct from other parts of the line (red arrow on Figure 4.16b). These points were dropped from the analysis. In Segment A, the first two picks were dropped from the analysis where part of the echogram is cutoff (red circle in Figure 4.15b). We also found an erroneous pick on the top layer, so this point was removed as well.

Table 4.3: Average picked snow depth and uncertainty values for each segment averaged across the number of points, N.

Segment	N	avg snow depth	uncertainty	COV
A	37	1.15 m	0.21 m	18.2%
B	121	1.13 m	0.20 m	17.3%
C	26	1.17 m	0.22 m	18.7%
D	29	1.25 m	0.20 m	16.1%

It should be noted that certain areas of the echogram were not clear for picking discernible snow top and bottom layers. Segment C shows several areas (red and black squares in Figure 4.17b)

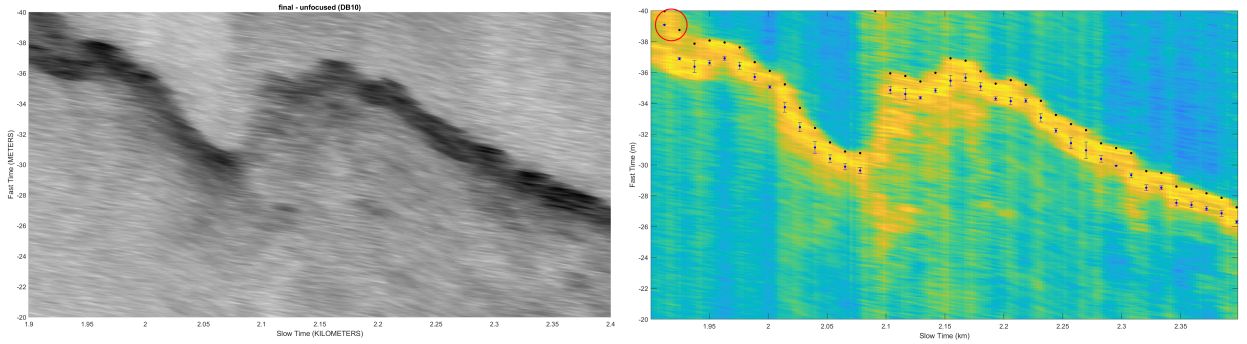

(a) Raw Echogram (b) Filtered and Picked Echogram

Figure 4.15: (a) Raw echogram of Segment A. (b) Smoothed and Sharpened echogram by convolution with picked locations of the snow top and snow bottom with uncertainty of the bottom layer Shown with error bars. The red circle indicates were points were dropped from the analysis due to cutoff, along with an erroneous pick at the top of the graph near x=2.1.

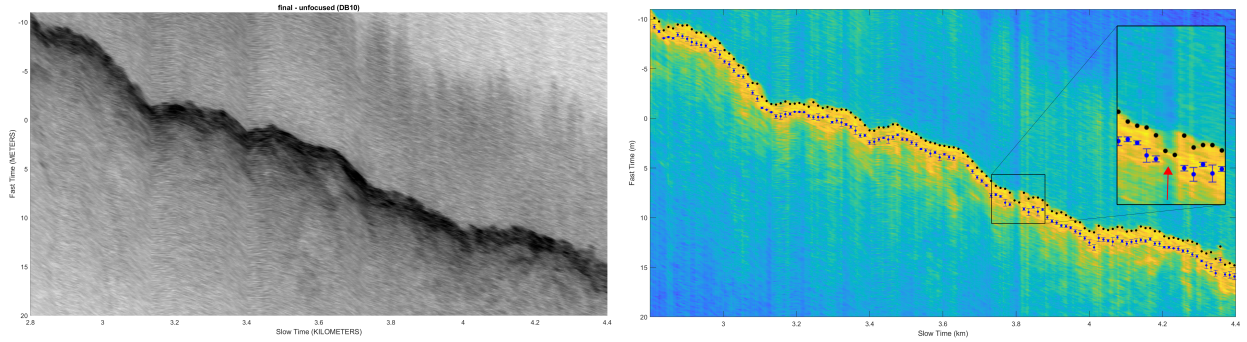

(a) Raw Echogram (b) Filtered and Picked Echogram

Figure 4.16: Similar to Figure 4.15 but for Segment B. The main highway is visible in (b) near x=3.8 (red arrow).

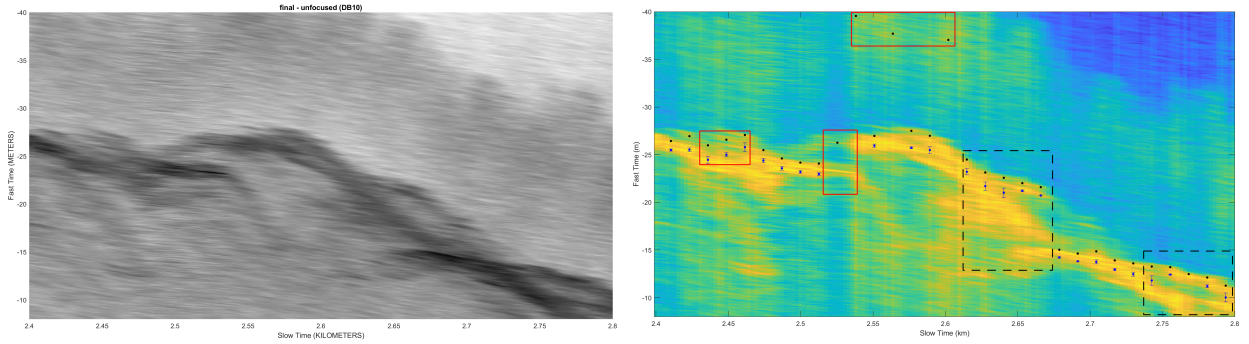

(a) Raw Echogram (b) Filtered and Picked Echogram

Figure 4.17: Similar to Figure 4.15 but for Segment C. Red squares indicate problem areas of picks that were dropped from the analysis. The blacked dashed squares indicate high uncertainty to accurately pick out the top and bottom of the snowpack.

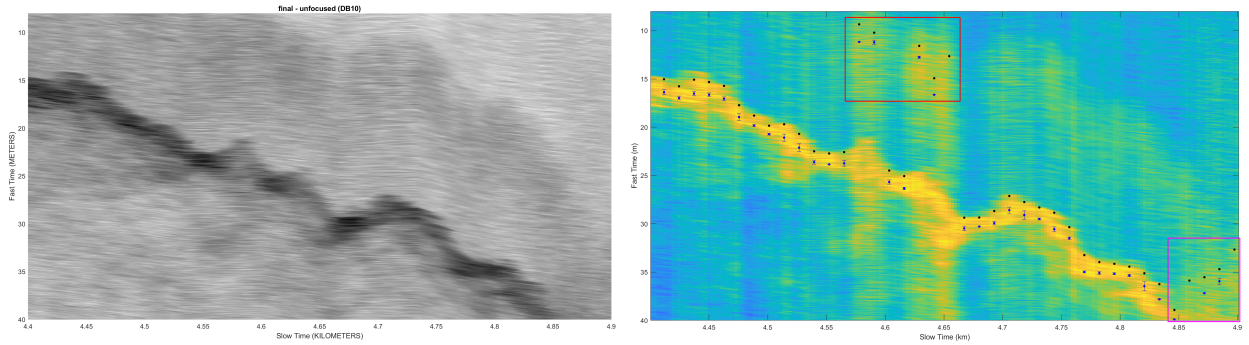

(a) Raw Echogram (b) Filtered and Picked Echogram

Figure 4.18: Similar to Figure 4.15 but for Segment D. Red and magenta boxes show were picks were dropped from the analysis due to picking errors.

where picking a top and bottom layer is difficult despite smoothing and sharpening. However, we were still able to confidently obtain snow depths at most locations. Across 26 picks, the snow depths at segment C averaged around 1.17 m with an average uncertainty of 0.22 m (18.7% of the mean). Additionally with Segment D, erroneous picked locations were also removed from the analysis due to wrong pick locations (red square on Figure 4.18b) and due to cutoff (magenta square on Figure 4.18b). For Segment D, we were able to get 29 picks with an average snow depth of 1.25 m with an average uncertainty of 0.20 m (16.1% of the mean). Segment C remains the hardest to pick, with discontinuities and more surface noise compared to the other segments.

Explaining the differences between the segments, we compared the physical environments of

the flightline segments. The canopy and elevation profiles for the ground projection flightline are shown on Figure 4.19. We see that elevations are relatively consistent across 3 out of the 4 segments. Segment D has the greatest difference in elevation change. Segments C and D also have higher tree canopy coverage percentages. Segments A and B have greater changes in tree canopy cover, but is on average lower compared to Segments C and D. To see what effects these variables had, correlation metrics are reported. Figure 4.20 shows the Pearson and Spearman Rank correlations between picked snow depths and corresponding environmental conditions using geolocated points from a (Keyhole Markup Language) KML Google Earth file provided by the University of Alabama. Across all of the segments, all variables are weakly anti-correlated with TCC, elevation, slope, roughness and TRI. However, confidence in correlations with picked snow depths are relatively low, with p-values all greater than 0.1. These relationships does not change, with the exception of two segments. Segment B has a Pearson correlation of -0.570 (p-value: 0.0265) and a Spearman Rank correlation of -0.565 (pvalue = 0.02823). These values were only obtained by ignoring TCC values of 0. The other weakly anti-correlated relationship was found in segment D between picked snow depths and elevation with a Pearson correlation of -0.801 (p-value = 0.0304). Correlation results for the picked uncertainty was very similar. Generally, most relationships had fairly low confidence with p-values greater than 0.1. The three significant correlations results were between TCC and uncertainty in segments A and B. Only Spearman Rank correlations had any significance with correlation=-0.750 (p-value=0.0522) with 0% TCC included and correlation = -0.771 (p-value = 0.0724) with 0% TCC removed in segment A. The correlation was -0.540 (p-value = 0.0379).

Table 4.4: Average values for each segments for tree canopy cover, slope, Roughness, and TRI.

Segment	**TCC**	**Slope**	**Roughness**	**TRI**
A	32.4%	6.65	1.03	0.28
B	19.0%	4.86	0.67	0.20
C	34.2%	3.93	0.57	0.18
D	36.6%	10.7	1.48	0.49

Examining the aspect along the flight line, the data were first split into four categories by the 4

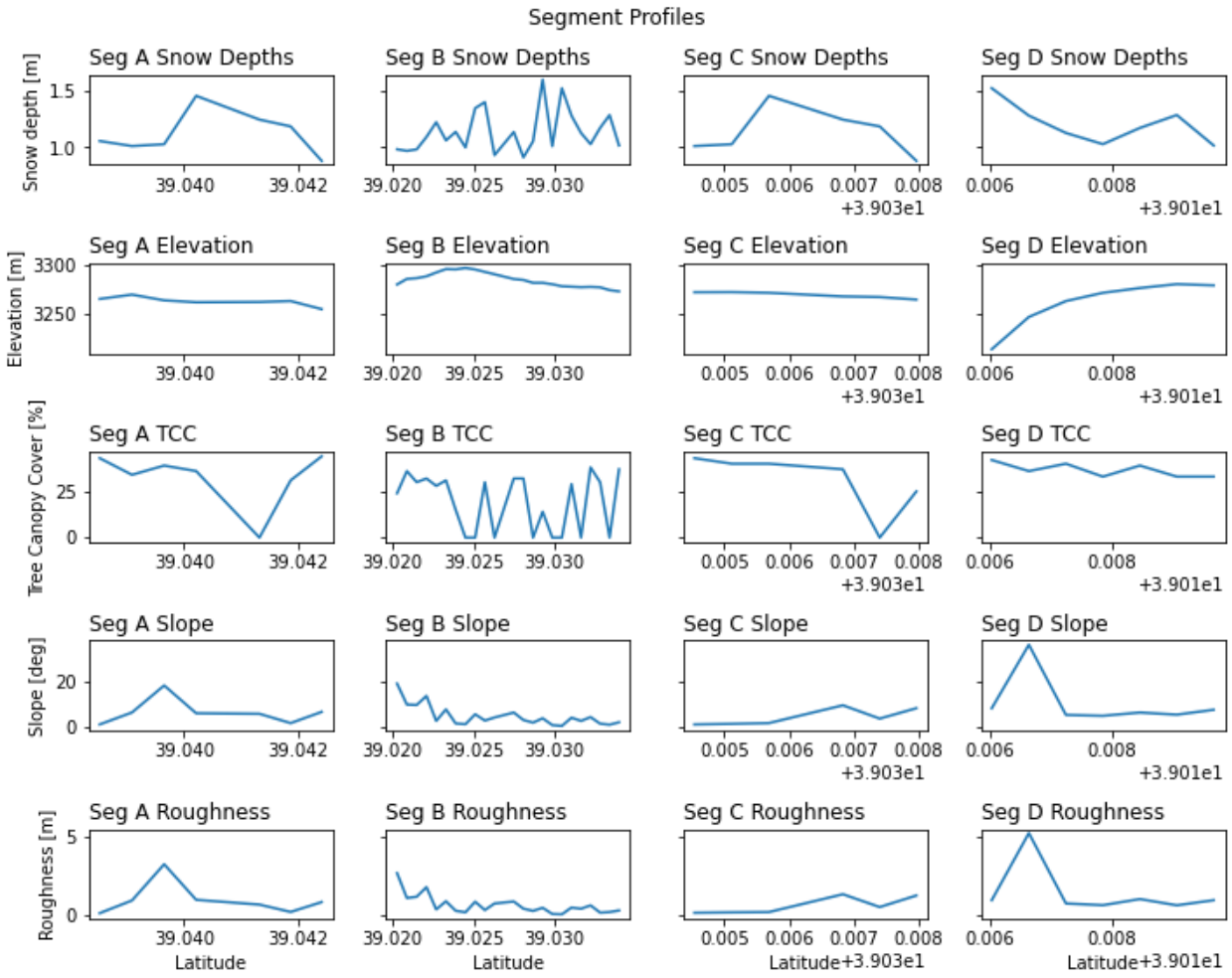

Figure 4.19: Profiles for each segment separated by column and variables by row. The profile is plotted by latitude so the North is situated to the right, opposite of the echogram orientation.

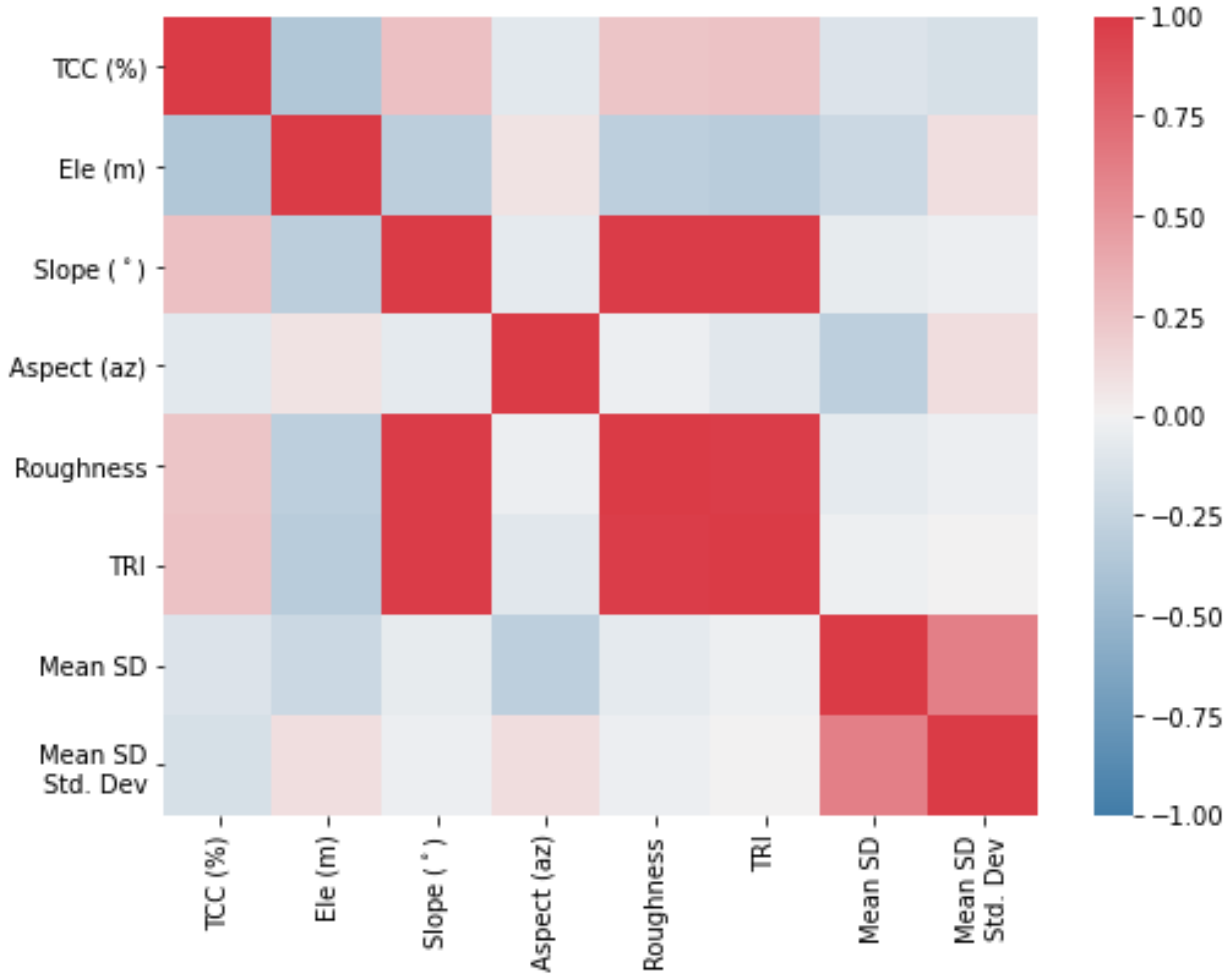

Figure 4.20: Correlation chart between physical environmental variables and picked snow depth and picked snow depth uncertainty. Slopes are highly correlated with roughness metrics(Roughness and TRI). Snow depths appear to be mostly weakly anti-correlated or weakly correlated with most variables, while uncertainties are very weakly anti-correlated with exception to elevation and aspect. All p-values for these Pearson correlation values have little to no confidence.

cardinal direction. Figure 4.21 shows whether the aspect played any part in changing picked snow depths or picked uncertainty. Across all of the segments, the lowest snow depths were found on slopes between 180 and 270 degrees. The southern facing slopes should receive more sunlight in the winter. These values would also be attenuated by other factors like slope, canopy cover, and wind - which was not within the scope of this thesis. To determine whether changes in aspect may play a role in echograms segments with noise, we also compared differences in the uncertainty levels with respect to aspect direction. However, the uncertainty levels did not appear to change with azimuth directions as all median and mean values were around .20 m. Comparing profiles of aspect on the ground projected flight line shows the most change in aspect occurred in Segment A and B.

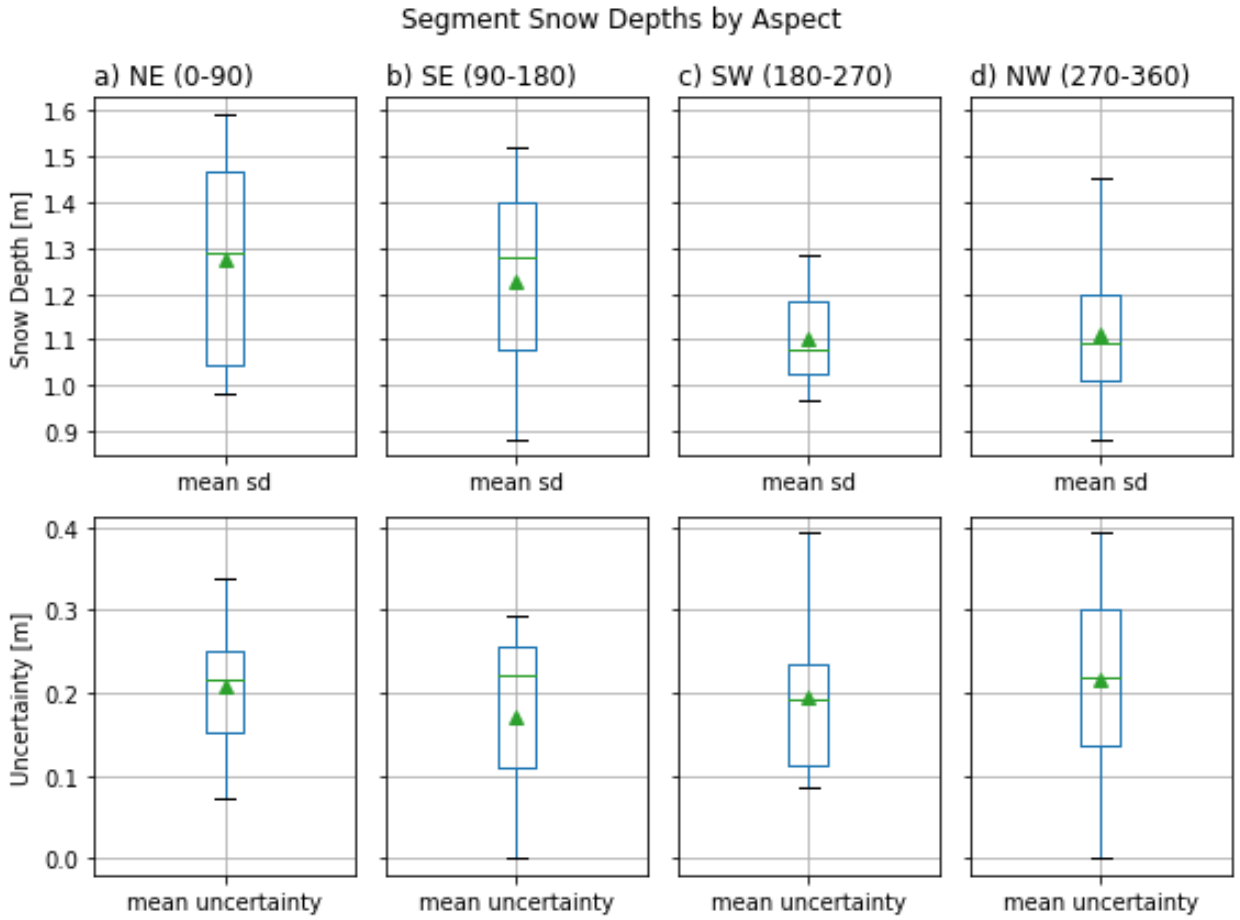

Figure 4.21: Boxplots showing distributions of snow depths (top row) and snow depth uncertainty (bottom row) from radar measurements. The aspect was divided by a) between N and E (0-90), b) between E and S (90-180), c) between S and W (180-270) and d) between W and N (270-360).

Chapter 5

Discussion and Conclusions

By aggregating in situ measurements to simulate a 7m by 70 m radar footprint, we have quantified the amount of natural variability of snow depths that can be used to benchmark uncertainty metrics of radar derived snow depths. Snow depths at these scale length can vary by on average 20% (generally 5% to 30%) of the mean over Grand Mesa. Outside of temporal factors, elevation, canopy height, and tree canopy cover are the best features in determining snow depths as shown in the previous literature, and are the top variables found by this study for modelling snow depths using a randomforest regression. When comparing these results to radar derived snow depths, we can conclude the following:

1. Bounding the picking algorithm by locally derived upper and lower bounds for the bottom layer of the snowpack produces results that are fairly consistent to each other. However, all values were well within the levels of natural snow depth variability.

2. Tree canopy cover is potentially the best explanation for radar derived snow depths and its uncertainty. In the 6 km segment that was currently available, tree canopy cover produced the most probable reason for the anti-correlations in snow depth values and its uncertainty. However, there needs to be further investigation as other flightlines become available for analysis in the future,

Previous Snow Radar measurements of snow depths from February 16, 2016 over Grand Mesa were measured to be between 1.07 to 1.62 m (Yan et al., 2016a). In comparison, the Mesa Lakes and Park Reservoir SNOTEL stations reported a snow thickness of 1.17 m and 1.47 m respectively (Yan et al., 2016a). In January 30, 2020, our radar-derived snow depths varied between 0.80 m and

1.59 m, with SNOTEL measurements at Mesa Lakes and Park Reservoirs reporting snow depths of 0.89 m and 1.24 m respectively. The MBE for the 2020 radar-derived snow depths are -0.26 m and 0.1 m compared to the Mesa Lakes and Park Reservoir stations respectively. Compared to the CReSIS20 errors statistics on Table 3.4 which were located in roughly the same area, we also observed daily MBE of -0.2 m (Mesa Lakes) and 0.17 m (Park Reservoir) against SNOTEL measurements. The similarity against both of these measurements with a simple picking algorithm suggests broad good agreements with the 2020 radar-derived measurements.

Trends of the relations between snow depth distribution and topological features and canopy structures agreed with previous literature. We have observed increasing snow depths with elevation on Grand Mesa which agrees with prior studies about elevation (e.g., (Dingman, 1981), (Elder et al., 1991), (Grünewald et al., 2014)). From 2017 lidar-based snow depth measurements from Grand Mesa, under-canopy snow depths were notable shallower within large canopy clusters, with a pronounced increase in snow depths over the transition between under-canopy to open conditions, before reaching a maximum under fully open conditions (Mazzotti et al., 2019). We have noted a similar relationship between our in situ snow depth measurements and canopy areas. However, changes in meteorological patterns, wind-driven redistribution, and changes to incoming/outgoing solar radiation which will vary throughout the snow season are all important processes to account.

Many errors in picks were largely caused by either an erroneous pick of the snow top layer or the lack of strong returns where we expect the snow bottom layer to be. Picking errors of the snow top is largely caused by strong returns from the canopy layer which was exaggerated by the standardization of the data matrix as seen in Segments A, C, D. To remedy this problem, sub-banding the Snow Radar measurements may help to reduce algorithms from picking the canopy layer. Echograms which were sub-banded to 2-4 GHz (Figure 5.1) notably lack the darker grey area above the snow top layer or air-snow interface that we observed with echograms provided in this study (see Figure 3.9 and Figures 4.15a-4.18a). Experimenting with different sub-bands may help not only to pick accurate snow depths, but also help to make internal layers more visible, or include canopy detection within the picking algorithm to discern differences between radar returns

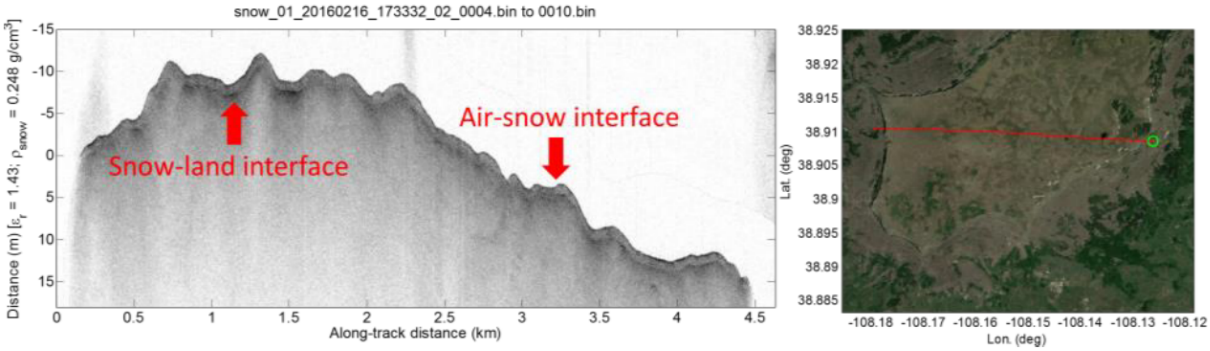

Figure 5.1: An example of a Snow Radar echogram sub-banded to 2-4 GHz, with its relative location from Grand Mesa to the right from Yan et al. (2016a). Notice the lack of a visible tree canopy layer in this echogram above the air-snow interface.

for snow under different canopy structures.

5.1 Future Work

Future work shows that additional fieldwork in Grand Mesa especially in forested areas is needed. Our CReSIS field campaign largely measured snow depths in open regions. The SnowEx measurements helped to alleviate this issue with snow depths measured across multiple canopy heights and tree canopy cover. Still, the number of open measurements exceeds the number of measurements made under the canopy (23,000 vs 14000). Ideally, we would like to obtain geolocated in situ measurements of snow depths under a variety of canopy conditions to ascertain true trends. Other relationships we can consider are how the canopy also affects snow density and snow wetness and model how these changes can affect radar returns. From some of the snow pit measurements in 2019 and our snow tube measurements in 2020, the average snow density was 314.8 kg m^{-3} and 182.7 kg m^{-3} respectively. Additionally, comparing observations at multiple times during the year - i.e. measurements in January and March in the same year may also help answer questions on snow depth variability as the snowpack matures, as well as maybe being crucial to identifying distinct layers in the snowpack as well. A campaign in January and March of the same water year may show that snow depth variability does reduce as we approach early spring due to warmer temperatures or melting.

Although it was mentioned throughout this study, the impacts of wind and wind blown snow were not quantified. While the strengthening of correlation metrics and the various studies (e.g. Currier & Lundquist, 2018) shows there is some effect, how much this affects snow depths were not examined. This wind blown metric may also be added to the RF regression in order to improve the predicted values. Other variables that are also considered are surface aspect, precipitation, and energy balances of insolation and sublimation are variables to consider for updating this regression model.

Future work also needs to be on obtaining more radar data in the 2019 and 2020 campaigns to analyze. The small data that was presented in this study shows some results that need further data to fully answer. Continued development of the picking algorithm is needed, but even robust results as provided here can produce results that exhibit similar levels of uncertainty as seen in the natural environment.

References

Bales, R. C., Molotch, N. P., Painter, T. H., Dettinger, M. D., Rice, R., & Dozier, J. (2006). Mountain hydrology of the western United States. *Water Resources Research*, 42(8).

Barnett, T. P., Adam, J. C., & Lettenmaier, D. P. (2005). Potential impacts of a warming climate on water availability in snow-dominated regions.

Behrangi, A., Bormann, K. J., & Painter, T. H. (2018). Using the Airborne Snow Observatory to Assess Remotely Sensed Snowfall Products in the California Sierra Nevada. *Water Resources Research*, 54(10), 7331–7346.

Blum, A. G. & Miller, A. (2019). Opportunities for forecast-informed water resources management in the United States. *Bulletin of the American Meteorological Society*, 100(10), 2087–2090.

Bormann, K. J., Westra, S., Evans, J. P., & McCabe, M. F. (2013). Spatial and temporal variability in seasonal snow density. *Journal of Hydrology*, 484, 63–73.

Breiman, L. (2001). Random forests. *Machine Learning*, 45(1), 5–32.

Carroll, T. (2001). Airborne Gamma Radiation Snow Survey Program: A user's guide, version 5.0. *National Operation Hydrologic Remote Sensing Center*, (pp. 1–14).

Carroll, T., Cline, D., Olheiser, C., Rost, A., Nilsson, A., Fall, G., Bovitz, C., & Li, L. (2006). Noaa's national snow analyses. In *Proceedings of the 74th annual meeting of the Western Snow Conference*, volume 74 (pp.1̃3).

Cho, E., Jacobs, J. M., & Vuyovich, C. M. (2020). The Value of Long-Term (40 years) Airborne Gamma Radiation SWE Record for Evaluating Three Observation-Based Gridded SWE Data Sets by Seasonal Snow and Land Cover Classifications. *Water Resources Research*, 56(1).

Clow, D. W., Nanus, L., Verdin, K. L., & Schmidt, J. (2012). Evaluation of SNODAS snow depth and snow water equivalent estimates for the Colorado Rocky Mountains, USA. *Hydrological Processes*, 26(17), 2583–2591.

Coulston, J. W., Moisen, G. G., Wilson, B. T., Finco, M. V., Cohen, W. B., & Brewer, C. K. (2012). Modeling percent tree canopy cover: A pilot study. *Photogrammetric Engineering and Remote Sensing*, 78(7), 715–727.

Currier, W. R. & Lundquist, J. D. (2018). Snow Depth Variability at the Forest Edge in Multiple Climates in the Western United States. *Water Resources Research*, 54(11), 8756–8773.

Deems, J. S., Painter, T. H., & Finnegan, D. C. (2013). Lidar measurement of snow depth: A review.

Dettinger, M., Udall, B., & Georgakakos, A. (2015). Western water and climate change. *Ecological Applications*, 25(8), 2069–2093.

Dingman, S. L. (1981). Elevation: A major influence on the hydrology of new hampshire and vermont, usa. *Hydrological Sciences Bulletin*, 26(4), 399–413.

Diro, G. T. & Sushama, L. (2020). Contribution of Snow Cover Decline to Projected Warming Over North America. *Geophysical Research Letters*, 47(1), 1–9.

Doesken, N. & Judson, A. (1997). The Snow Booklet.

Dressler, K. A., Fassnacht, S. R., & Bales, R. C. (2006). A Comparison of Snow Telemetry and Snow Course Measurements in the Colorado River Basin. *Journal of Hydrometeorology*, 7(4), 705–712.

Elder, K., Dozier, J., & Michaelsen, J. (1989). Spatial and Temporal Variation of Net Snow Accumulation in a Small Alpine Watershed, Emerald Lake Basin, Sierra Nevada, California, U.S.A. *Annals of Glaciology*, 13(October 2017), 56–63.

Elder, K., Dozier, J., & Michaelsen, J. (1991). Snow accumulation and distribution in an Alpine Watershed. *Water Resources Research*, 27(7), 1541–1552.

Fassnacht, S. R., Dressler, K. A., & Bales, R. C. (2003). Snow water equivalent interpolation for the Colorado River Basin from snow telemetry (SNOTEL) data. *Water Resources Research*, 39(8).

Grünewald, T., Bühler, Y., & Lehning, M. (2014). Elevation dependency of mountain snow depth. *Cryosphere*, 8(6), 2381–2394.

Guyennon, N., Valt, M., Salerno, F., Petrangeli, A. B., & Romano, E. (2019). Estimating the snow water equivalent from snow depth measurements in the Italian Alps. *Cold Regions Science and Technology*, 167, 102859.

Hedrick, A. R., Marks, D., Havens, S., Robertson, M., Johnson, M., Sandusky, M., Marshall, H. P., Kormos, P. R., Bormann, K. J., & Painter, T. H. (2018). Direct Insertion of NASA Airborne Snow Observatory-Derived Snow Depth Time Series Into the iSnobal Energy Balance Snow Model. *Water Resources Research*, 54(10), 8045–8063.

Hiemstra, C., Marshall, H.-P., Vuyovich, C., Elder, K., Mason, M., & Durand, M. (2020). Snowex20 community snow depth probe measurements, version 1.

IPCC (2019). *The Ocean and Cryosphere in a Changing Climate. A Special Report of the Intergovernmental Panel on Climate Change*. Technical report.

Jin, S., Homer, C., Yang, L., Danielson, P., Dewitz, J., Li, C., Zhu, Z., Xian, G., & Howard, D. (2019). Overall methodology design for the United States national land cover database 2016 products. *Remote Sensing*, 11(24).

Johnson, J. B. & Marks, D. (2004). The detection and correction of snow water equivalent pressure sensor errors. *Hydrological Processes*, 18(18), 3513–3525.

Johnson, J. B. & Schaefer, G. L. (2002). The influence of thermal, hydrologic, and snow deformation mechanisms on snow water equivalent pressure sensor accuracy. *Hydrological Processes*, 16(18), 3529–3542.

Jonas, T., Marty, C., & Magnusson, J. (2009). Estimating the snow water equivalent from snow depth measurements in the Swiss Alps. *Journal of Hydrology*, 378(1-2), 161–167.

Kim, E., Gatebe, C., Hall, D., Newlin, J., Misakonis, A., Elder, K., Marshall, H. P., Hiemstra, C., Brucker, L., De Marco, E., Crawford, C., Kang, D. H., & Entin, J. (2017). NASA's snowex campaign: Observing seasonal snow in a forested environment. *International Geoscience and Remote Sensing Symposium (IGARSS)*, 2017-July, 1388–1390.

Knowles, N., Dettinger, M. D., & Cayan, D. R. (2006). Trends in snowfall versus rainfall in the western United States. *Journal of Climate*, 19(18), 4545–4559.

Li, D., Wrzesien, M. L., Durand, M., Adam, J., & Lettenmaier, D. P. (2017). How much runoff originates as snow in the western United States, and how will that change in the future? *Geophysical Research Letters*, 44(12), 6163–6172.

Lievens, H., Demuzere, M., Marshall, H. P., Reichle, R. H., Brucker, L., Brangers, I., de Rosnay, P., Dumont, M., Girotto, M., Immerzeel, W. W., Jonas, T., Kim, E. J., Koch, I., Marty, C., Saloranta, T., Schöber, J., & De Lannoy, G. J. (2019). Snow depth variability in the Northern Hemisphere mountains observed from space. *Nature Communications*, 10(1).

López-Moreno, J. I., Fassnacht, S. R., Heath, J. T., Musselman, K. N., Revuelto, J., Latron, J., Morán-Tejeda, E., & Jonas, T. (2013). Small scale spatial variability of snow density and depth over complex alpine terrain: Implications for estimating snow water equivalent. *Advances in Water Resources*, 55, 40–52.

Malle, J., Rutter, N., Mazzotti, G., & Jonas, T. (2019). Shading by Trees and Fractional Snow Cover Control the Subcanopy Radiation Budget. *Journal of Geophysical Research: Atmospheres*, 124(6), 3195–3207.

Marshall, H. P., Koh, G., Sturm, M., Johnson, J. B., Demuth, M., Landry, C., Deems, J. S., & Gleason, J. A. (2006). Spatial variability of the snowpack: Experiences with measurements at a wide range of length scales with several different high precision instruments. In *Proceedings ISSW 2006. International Snow Science Workshop, Telluride CO, U.S.A., 1-6 October 2006*, number June 2016 (pp. 359–364).

Marshall, H. P., Schneebeli, M., & Koh, G. (2007). Snow stratigraphy measurements with high-frequency FMCW radar: Comparison with snow micro-penetrometer. *Cold Regions Science and Technology*, 47(1-2 SPEC. ISS.), 108–117.

Mazzotti, G., Currier, W. R., Deems, J. S., Pflug, J. M., Lundquist, J. D., & Jonas, T. (2019). Revisiting Snow Cover Variability and Canopy Structure Within Forest Stands: Insights From Airborne Lidar Data. *Water Resources Research*, 55(7), 6198–6216.

McCabe, G. J., Clark, M. P., & Hay, L. E. (2007). Rain-on-snow events in the western United States. *Bulletin of the American Meteorological Society*, 88(3), 319–328.

McGrath, D., Webb, R., Shean, D., Bonnell, R., Marshall, H., Painter, T. H., Molotch, N. P., Elder, K., Hiemstra, C., & Brucker, L. (2019). Spatially extensive ground-penetrating radar snow depth observations during NASA's 2017 SnowEx Campaign: Comparison with in situ, airborne, and satellite observations. *Water Resources Research*, 55(11), 10026–10036.

Mote, P. W., Hamlet, A. F., Clark, M. P., & Lettenmaier, D. P. (2005). Declining mountain snowpack in western north America. *Bulletin of the American Meteorological Society*, 86(1), 39–49.

Musselman, K. N., Molotch, N. P., & Brooks, P. D. (2008). Effects of vegetation on snow accumulation and ablation in a mid-latitude sub-alpine forest. *Hydrological Processes*, 22(15), 2767–2776.

Oaida, C. M., Reager, J. T., Andreadis, K. M., David, C. H., Levoe, S. R., Painter, T. H., Bormann, K. J., Trangsrud, A. R., Girotto, M., & Famiglietti, J. S. (2019). A high-resolution data assimilation framework for snow water equivalent estimation across the Western United States and validation with the Airborne Snow Observatory. *Journal of Hydrometeorology*, 20(3), 357–378.

Painter, T. H., Berisford, D. F., Boardman, J. W., Bormann, K. J., Deems, J. S., Gehrke, F., Hedrick, A., Joyce, M., Laidlaw, R., Marks, D., Mattmann, C., McGurk, B., Ramirez, P., Richardson, M., Skiles, S. M. K., Seidel, F. C., & Winstral, A. (2016). The Airborne Snow Observatory: Fusion of scanning lidar, imaging spectrometer, and physically-based modeling for mapping snow water equivalent and snow albedo. *Remote Sensing of Environment*, 184, 139–152.

Painter, T. H., Berisford, D. F., Boardman, J. W., Bormann, K. J., Deems, J. S., Gehrke, F., Joyce, M., Laidlaw, R., Mattmann, C., McGurk, B., Ramirez, P., Richardson, M., & Skiles, S. M. (2020). Aso l4 lidar point cloud digital terrain model 3m utm grid, version 1.

Panzer, B., Gomez-Garcia, D., Leuschen, C., Paden, J., Rodriguez-Morales, F., Patel, A., Markus, T., Holt, B., & Gogineni, P. (2013). An ultra-wideband, microwave radar for measuring snow thickness on sea ice and mapping near-surface internal layers in polar firn. *Journal of Glaciology*, 59(214), 244–254.

Pedregosa, F., Varoquaux, G., Gramfort, A., Michel, V., Thirion, B., Grisel, O., Blondel, M., Prettenhofer, P., Weiss, R., Dubourg, V., Vanderplas, J., Passos, A., Cournapeau, D., Brucher, M., Perrot, M., & Duchesnay, E. (2011). Scikit-learn: Machine learning in Python. *Journal of Machine Learning Research*, 12, 2825–2830.

Potapov, P., Li, X., Hernandez-Serna, A., Tyukavina, A., Hansen, M. C., Kommareddy, A., Pickens, A., Turubanova, S., Tang, H., Silva, C. E., Armston, J., Dubayah, R., Blair, J. B., & Hofton, M. (2021). Mapping global forest canopy height through integration of GEDI and Landsat data. *Remote Sensing of Environment*, 253, 112165.

Reidmiller, D. R., Avery, C. W., Easterling, D. R., Kunkel, K. E., Lewis, K. L. M., Maycock, T. K., & Stewart, B. C. (2018). Impacts, Risks, and Adaptation in the United States: Fourth National Climate Assessment, Volume II.

Seager, R., Ting, M., Held, I., Kushnir, Y., Lu, J., Vecchi, G., Huang, H. P., Harnik, N., Leetmaa, A., Lau, N. C., Li, C., Velez, J., & Naik, N. (2007). Model projections of an imminent transition to a more arid climate in southwestern North America. *Science*, 316(5828), 1181–1184.

Serreze, M. C., Clark, M. P., Armstrong, R. L., McGinnis, D. A., & Pulwarty, R. S. (1999). Characteristics of the western United States snowpack from snowpack telemetry (SNOTEL) data. *Water Resources Research*, 35(7), 2145–2160.

Sexstone, G. A., Clow, D. W., Fassnacht, S. R., Liston, G. E., Hiemstra, C. A., Knowles, J. F., & Penn, C. A. (2018). Snow Sublimation in Mountain Environments and Its Sensitivity to Forest Disturbance and Climate Warming. *Water Resources Research*, 54(2), 1191–1211.

Stewart, I. T., Cayan, D. R., & Dettinger, M. D. (2005). Changes toward earlier streamflow timing across western North America. *Journal of Climate*, 18(8), 1136–1155.

Strasser, U., Bernhardt, M., Weber, M., Liston, G. E., & Mauser, W. (2008). Is snow sublimation important in the alpine water balance? *Cryosphere*, 2(1), 53–66.

Sturm, M., Goldstein, M. A., & Parr, C. (2017). Water and life from snow: A trillion dollar science question.

Sturm, M. & Holmgren, J. (2018). An Automatic Snow Depth Probe for Field Validation Campaigns. *Water Resources Research*, 54(11), 9695–9701.

Sturm, M., Taras, B., Liston, G. E., Derksen, C., Jonas, T., & Lea, J. (2010). Estimating Snow Water Equivalent Using Snow Depth Data and Climate Classes. *Journal of Hydrometeorology*, 11(6), 1380–1394.

Taylor, R. A., Gogineni, S., Gurbuz, S., Kolpuke, S., Li, L., Neill, O., Yan, J.-b., Akins, T., Carswell, J., Braaten, D., & Tsutaki, S. (2019). A PROTOTYPE ULTRA-WIDEBAND FMCW RADAR FOR SNOW AND SOIL-MOISTURE MEASUREMENTS Remote Sensing Solutions , Barnstable , MA , USA Center for Remote Sensing of Ice Sheets , University of Kansas , Lawrence , KS , USA Atmosphere and Ocean Research Institute , T. *IGARSS 2019 - 2019 IEEE International Geoscience and Remote Sensing Symposium*, (pp. 3974–3977).

Tedesco, M. & Narvekar, P. S. (2010). Assessment of the NASA AMSR-E SWE Product. *IEEE Journal of Selected Topics in Applied Earth Observations and Remote Sensing*, 3(1), 141–159.

Yan, J. B., Gogineni, S., Braaten, D., Brozena, J., Rodriguez-Morales, F., & Arnold, E. (2016a). Ultra-wideband radars operating over the frequency range of 2-18 GHZ for measurements on terrestrial snow and ice. *International Geoscience and Remote Sensing Symposium (IGARSS)*, 2016-Novem, 7078–7081.

Yan, J. B., Gogineni, S., Camps-Raga, B., & Brozena, J. (2016b). A Dual-Polarized 2-18-GHz Vivaldi Array for Airborne Radar Measurements of Snow. *IEEE Transactions on Antennas and Propagation*, 64(2), 781–785.

Yan, J. B., Gogineni, S., Rodriguez-Morales, F., Gomez-Garcia, D., Paden, J., Li, J., Leuschen, C. J., Braaten, D. A., Richter-Menge, J. A., Farrell, S. L., Brozena, J., & Hale, R. D. (2017a). Airborne measurements of snow thickness: Using ultrawide-band frequency-modulated-continuous-wave radars. *IEEE Geoscience and Remote Sensing Magazine*, 5(2), 57–76.

Yan, J. B., Gomez-Garcia Alvestegui, D., McDaniel, J. W., Li, Y., Gogineni, S., Rodriguez-Morales, F., Brozena, J., & Leuschen, C. J. (2017b). Ultrawideband FMCW radar for airborne measurements of snow over sea ice and land. *IEEE Transactions on Geoscience and Remote Sensing*, 55(2), 834–843.

Yankielun, N., Rosenthal, W., & Davis, R. E. (2004). Alpine snow depth measurements from aerial FMCW radar. *Cold Regions Science and Technology*, 40(1-2), 123–134.

Zeng, X., Broxton, P., & Dawson, N. (2018). Snowpack Change From 1982 to 2016 Over Conterminous United States. *Geophysical Research Letters*, 45(23), 12,940–12,947.